

GENETIC REDUCTION OF CHOLESTEROL SYNTHESIS IN  
THE MOUSE BRAIN DOES NOT AFFECT AMYLOID  
FORMATION IN AN ALZHEIMER'S DISEASE  
MODEL, BUT DOES EXTEND LIFESPAN

APPROVED BY SUPERVISORY COMMITTEE

---

David W. Russell, Ph.D.

---

Thomas Sudhoff, M.D., Ph.D.

---

Kimberly Huber, Ph.D.

---

Craig Powell, Ph.D.

## **DEDICATION**

It is impossible for me to communicate in ink on paper the depth of the gratitude I feel toward all of the people in my life who provided support, encouragement and love to me throughout the years that it took to complete this project. There were countless roadblocks and obstacles, of both a personal and professional nature, that kept me from becoming too relaxed and often required charting of indirect paths towards goals on the horizon. I would like to believe that, just like a fitness course (or a war zone), the experiences that very clearly did not kill me have made me a stronger woman, more able to deal with the inevitable “curveballs” that will be thrown my way in the future. However, it would not have been possible for me to respect these experiences, good and bad, as opportunities for personal and intellectual growth had I not been blessed with the brilliant, wise and insightful people that lit this path and guided me along the way.

First and foremost, I would like to thank my mentor, David Russell, and the members of his laboratory. David, you set the standard to which all mentors should be held. You donated your time and energy to my success, pushed me without tipping me over, and you endured countless hours of torture, putting up with all of my nonsense. You are an experienced leader, a wise guide and a loyal friend and I am so lucky to have been a student under your instruction.

I would also like recognize the Medical Scientist Training Program and the Neuroscience Graduate Program, particularly Mike Brown, Rod Ulane, Dennis McKearin, Andrew Zinn, Robin Downing, Stephanie Robertson, Jane Johnson and my committee members, Thomas Sudhoff, Kimberly Huber and Craig Powell for their patience, flexibility, support and advice throughout my many years as a student in this program. They provided the scientific sounding board for my projects and ideas and worked hard to keep me focused on the task at hand, which was completion of the project that is the subject of this dissertation. Thank you.

Finally, I would like to dedicate this document and all of the migraine headaches, sleepless nights, beads of sweat, teardrops, blood (yes, blood!), frustration, heart and soul, favors, desperate emails, weekends in the animal colony and childlike enthusiasm that went into the development, execution and completion of this project to my parents, Linda and Garland Warren, my Grandma Bonnie and my two sisters, Melissa and Molly. There is not really much I could write that would serve my feelings justly. Fortunately, I trust that you will understand this because we share a closeness and understanding that defies words. You already know that without you, none of this would have been possible. As long as my heart is beating, I am in your debt and at your service, with love.

GENETIC REDUCTION OF CHOLESTEROL SYNTHESIS IN  
THE MOUSE BRAIN DOES NOT AFFECT AMYLOID  
FORMATION IN AN ALZHEIMER'S DISEASE  
MODEL, BUT DOES EXTEND LIFESPAN

by

REBEKKAH LYNN WARREN

DISSERTATION

Presented to the Faculty of the Graduate School of Biomedical Sciences

The University of Texas Southwestern Medical Center at Dallas

In Partial Fulfillment of the Requirements

For the Degree of

DOCTOR OF PHILOSOPHY

The University of Texas Southwestern Medical Center at Dallas

Dallas, Texas

March, 2009

Copyright

by

REBEKKAH LYNN WARREN, 2009

All Rights Reserved

GENETIC REDUCTION OF CHOLESTEROL SYNTHESIS IN  
THE MOUSE BRAIN DOES NOT AFFECT AMYLOID  
FORMATION IN AN ALZHEIMER'S DISEASE  
MODEL, BUT DOES EXTEND LIFESPAN

REBEKKAH LYNN WARREN, Ph.D.

The University of Texas Southwestern Medical Center at Dallas, 2009

DAVID RUSSELL, Ph.D.

In vitro alterations in cellular cholesterol content or synthesis affect the cleavage of amyloid precursor protein (APP) to amyloidogenic peptides characteristic of Alzheimer's disease (AD). To determine whether a decrease in cholesterol synthesis would affect APP processing in vivo, we crossed cholesterol 24-hydroxylase knockout (KO) mice, which exhibit a 50% reduction in sterol synthesis, with transgenic mice (B6.Cg-Tg(APP<sup>swe</sup>, PSEN1<sup>E9</sup>)85Dbo/J) that

develop AD and followed progression of the disease and lipid metabolism in the offspring. APP expression and amyloid plaque deposition in the cortex and hippocampus of 3- to 15-month-old male and female AD mice were similar in the presence and absence of cholesterol 24-hydroxylase. At 15 months of age, a modest but statistically significant decline in insoluble A $\beta$ <sub>40</sub> and A $\beta$ <sub>42</sub> peptide levels was detected in the hippocampus but not cortex of KO/AD mice versus WT/AD mice. Amyloid plaque accumulation did not affect brain sterol or fatty acid synthesis rates in 24-hydroxylase WT or KO mice. Unexpectedly, loss of one or two 24-hydroxylase alleles increased longevity in AD mice. These studies suggest that reducing de novo cholesterol synthesis in the brain will not substantially alter the course of AD, but may confer a survival advantage.

## TABLE OF CONTENTS

ABSTRACT .....	vi
PRIOR PUBLICATIONS .....	x
LIST OF FIGURES .....	xi
LIST OF ABBREVIATIONS .....	xii
INTRODUCTION .....	1
MATERIALS AND METHODS .....	24
I.    MOUSE MODEL .....	24
II.   TISSUE COLLECTION .....	26
III.  PLAQUE VISUALIZATION .....	28
a. SECTION PREPARATION .....	28
b. THIOFLAVINE S STAINING .....	29
c. CONGO RED STAINING .....	30
IV.  PLAQUE QUANTIFICATION .....	31
a. PILOT STUDY .....	31
b. THIOVLAVINE S V. CONGO RED .....	33
V.   A $\beta$ PEPTIDE QUANTIFICATION .....	35
a. TISSUE HOMOGENIZATION .....	35
b. PROTEIN ASSAY .....	36
c. QUANTITATIVE ELISA .....	37

VI.	IN VIVO CHOLESTEROL BIOSYNTHESIS .....	40
VII.	ANALYSIS OF PROTEINS RELATED TO CHOLESTEROL METABOLISM AND ALZHEIMER'S DISEASE .....	42
VIII.	SURVIVAL STUDY .....	45
	RESULTS .....	47
I.	PLAQUE ACCUMULATION IN AD MICE .....	47
II.	ANALYSIS OF PROTEINS RELATED TO CHOLESTEROL METABOLISM AND ALZHEIMER'S DISEASE .....	53
III.	QUANTIFICATION OF A $\beta$ PEPTIDES .....	56
IV.	IN VIVO CHOLESTEROL BIOSYNTHESIS .....	60
V.	SURVIVAL STUDY .....	63
	DISCUSSION .....	66
	BIBLIOGRAPHY .....	73

## PRIOR PUBLICATIONS

1. Yildiz Y, Matern H, Thompson B, Allegood JC, **Warren RL**, Ramirez DM, Hammer RE, Hamra FK, Matern S, & Russell DW (2006) *J Clin Invest* **116**, 2985-2994.
2. **Halford RW** & Russell DW (2009) *Proc Natl Acad Sci U S A* **106**, 3502-3506.

**LIST OF FIGURES**

FIGURE ONE .....	4
FIGURE TWO .....	18
FIGURE THREE .....	49
FIGURE FOUR .....	52
FIGURE FIVE .....	54
FIGURE SIX .....	58
FIGURE SEVEN .....	62
FIGURE EIGHT .....	65

**LIST OF ABBREVIATIONS**

<b>ABBREVIATION</b>	<b>DEFINITION</b>
24-Hydroxylase	Cholesterol 24-Hydroxylase
ABTS	2,2'-Azino-Bis(3-Ethylbenzothiazoline-6-Sulfonic Acid)
Acetyl CoA	Acetyl CoenzymeA
AD	Alzheimer's Disease
ADAM	A Disintegrin and Metalloproteinase
APLP	Amyloid Precursor-Like Protein
Apo	Apolipoprotein
APP	Amyloid Precursor Protein
A $\beta$	Amyloid- $\beta$ Peptide
BACE	$\beta$ -Site APP Cleavage Enzyme
BBB	Blood-Brain Barrier
BCA	Bicinchoninic Acid
CA	<i>Cornu Ammonis</i>
CCD	Charge-Coupled Device
cDNA	Complementary DNA
CL	Chemiluminescent
CNS	Central Nervous System

CSF	Cerebrospinal Fluid
DAB-1	Disabled
DAPI	4',6-Diamidino-2-Phenylindole
ddH <sub>2</sub> O	Double Distilled Water
DNA	Deoxyribonucleic Acid
dNTP	Deoxynucleoside Triphosphate
EDTA	Ethylenediaminetetraacetic Acid
ELISA	Enzyme-Linked Immunosorbent Assay
FAD	Familial Alzheimer's Disease
FH	Familial Hypercholesterolemia
GFAP	Glial Fibrillary Acid Protein
HBSS	Hank's Balanced Salt Solution
HDL	High-Density Lipoprotein
HET	Heterozygous
HMG CoA Reductase	3-Hydroxy-3-Methylglutaryl Coenzyme A Reductase
HRP	Horseradish Peroxidase
KO	Knock-out
LDL	Low-Density Lipoprotein
LRP	LDL Receptor Related Protein
LTP	Long-term Potentiation

LXR	Liver X Receptor
MAP	Microtubule Associated Protein
mRNA	Messenger RNA
NADPH	Nicotinamide Adenine Dinucleotide Phosphate
NFT	Neurofibrillary Tangle
NPC	Neimann-Pick C
P450	Cytochrome P450
PBS	Phosphate Buffered Saline
PBST	Phosphate Buffered Saline with 0.05% (v/v) Tween 20
PCR	Polymerase Chain Reaction
PFA	Paraformaldehyde
PNS	Peripheral Nervous System
Psen	Presenilin
PVDF	Polyvinylidene Difluoride
RIP	Regulated Intramembrane Proteolysis
RIPA	Radioimmunoprecipitation Assay
RNA	Ribonucleic Acid
RXR	Retinoid X Receptor
SD	Semi-Dry
SDS	Sodium Dodecyl Sulfate

SREBP	Sterol Regulatory Element Binding Protein
<i>Taq</i>	<i>Thermus aquaticus</i>
TBE	Tris-Borate-EDTA
TE	Tris-EDTA
UV	Ultraviolet
VLDL	Very Low-Density Lipoprotein
WT	Wild-type

## INTRODUCTION

It was known in the first half of the twentieth century that high circulating levels of cholesterol played a role in development of atherosclerosis and heart disease (1). Since then, intricate details of the pathways required for maintaining cholesterol homeostasis have been described. In the early 1970s, with studies of metabolic defects in patients with severe, heritable forms of hypercholesterolemia, Brown, Goldstein and colleagues began documenting the molecular events involved in cholesterol trafficking, sensing and regulation of the cholesterol biosynthetic pathway (2-4). The high degree of complexity and finesse with which cellular levels of this sterol are maintained parallels the lipid's importance to survival in eukaryotes.

Cholesterol is a necessary component of cellular membranes comprising as much as 25% of the lipid content of the mammalian plasma membrane. Cholesterol improves lipid packing, thereby decreasing membrane fluidity and permeability (5). The sterol also modulates the activity of proteins that exist within the plasma membrane, particularly those involved in cholesterol metabolism. In addition, cholesterol is utilized as a precursor in the generation of steroid hormones and bile acids, compounds important for long-range cellular communications and dietary lipid absorption, respectively.

The vertebrate nervous system is also highly enriched in cholesterol. Although the human brain accounts for only 2% of total body weight, it contains almost 25% of the body's pool of unesterified cholesterol (6). Importantly, cholesterol is the major lipid component of myelin sheaths, layered membrane processes elaborated by oligodendrocytes in the central nervous system (CNS) and Schwann cells in the peripheral nervous system (PNS). These highly specialized membranes insulate axons, reducing membrane capacitance and increasing resistance. These properties allow for rapid conduction of action potentials over considerable distances. As expected, cholesterol rapidly accumulates in the mammalian CNS during the period of active myelination in nervous system development. In addition to myelin sheaths, 20-30% of CNS cholesterol is found in the cell membranes of neurons and non-neuronal support cells, where it is thought to comprise an actively metabolized cholesterol pool (7).

In order to meet cholesterol needs, organisms can obtain cholesterol by two means: diet and *de novo* synthesis. Dietary cholesterol (in the form of chylomicrons) is transported to the liver via the circulation. *En route* to and away from the liver, chylomicrons are converted to cholesterol-rich remnants, a consequence of interaction with endothelial lipoprotein lipase, which hydrolyzes triglycerides into free fatty acids and glycerol. The liver takes up these remnants, as well as low-density lipoproteins (LDL) and very low-density lipoprotein (VLDL) remnants, through receptor-mediated endocytosis facilitated primarily by

the LDL receptor. Cholesterol acquired in this way can be used to carry out cellular functions or can be packaged into new lipoprotein particles, predominately VLDL. The latter particles are excreted into the circulation for use by peripheral tissues, particularly those that are highly metabolically active or are involved in steroid hormone biosynthesis. Like the liver, peripheral tissues are able to take up LDL cholesterol through receptor-mediated endocytosis; however, only about 20% of circulating LDL cholesterol is utilized by extrahepatic organs and the remainder is returned to the liver (7).

All nucleated cells are also capable of synthesizing cholesterol *de novo*. Despite the fact that the liver synthesizes and excretes large amounts of the sterol, peripheral tissues appear to acquire the majority of their cholesterol via synthesis (7). Cholesterol is produced from acetate via a 20-step biosynthetic pathway termed the 'mevalonate pathway' (Figure 1, modified from (8)). The rate-limiting step in this pathway is catalyzed by 3-hydroxy-3-methylglutaryl coenzyme A reductase (HMG CoA reductase). The expression and activity of this enzyme are under tight regulatory control dictated by cellular cholesterol content (9). Statins, a class of pharmacological agents that competitively inhibit HMG CoA reductase effectively reduce hepatic cholesterol synthesis and lower plasma levels of LDL via a compensatory increase in LDL receptors (10).

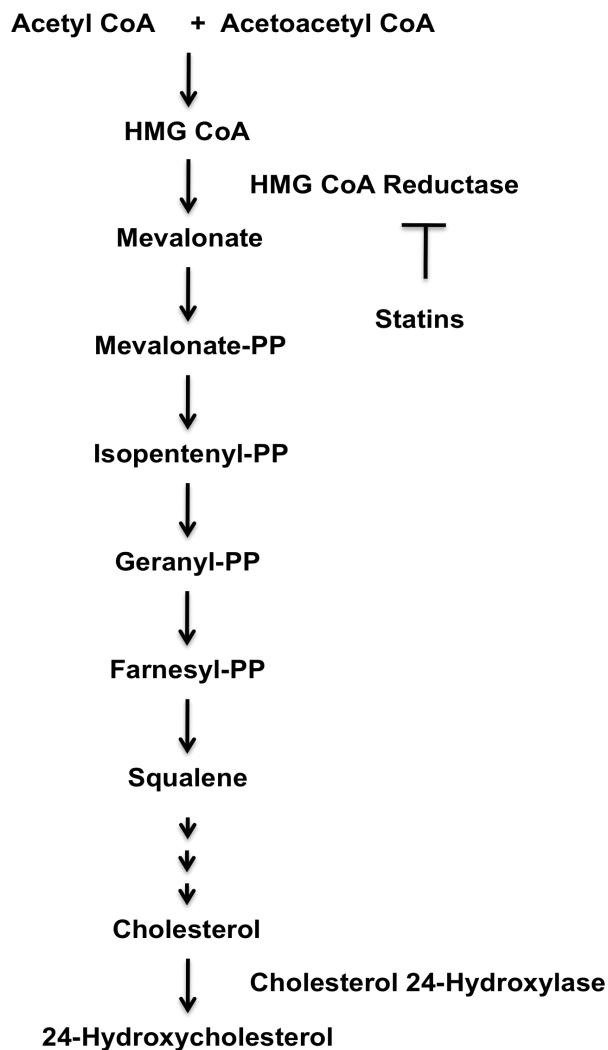


**Figure 1. Diagram of the cholesterol biosynthetic pathway.** Acetyl CoA is utilized to synthesize HMG CoA, a precursor molecule to isoprenoids and cholesterol. The conversion of HMG CoA to mevalonate represents the rate-limiting step in the pathway. The enzyme responsible for this reaction, HMG CoA Reductase, is the target of the cholesterol-lowering agents known as statins. Cholesterol excretion from the brain occurs through hydroxylation to 24-hydroxycholesterol, a reaction catalyzed by cholesterol 24-hydroxylase. Modified from (8).

Cholesterol levels in the organism are tightly maintained at a constant level (approximately 2,200 mg/kg body weight in mammals); therefore, it is necessary for cholesterol acquisition to be matched by an equivalent rate of excretion. The rate of cholesterol turnover for a given species is proportional to the animal's basal metabolic rate and can vary considerably among organs within the same animal (7). In general, cholesterol that accumulates in peripheral tissues is shed through the outer membrane leaflet of cells via association with ApoA-I containing HDL particles returning to the liver. Cholesterol can also be moved by ABC transporters in the liver and intestinal lumen or following conversion to water-soluble hydroxylated species by various sterol hydroxylating enzymes (7). Conversion to bile acids constitutes the major pathway for cholesterol excretion from the body, accounting for approximately 90% of the actively metabolized cholesterol pool. This pathway is initiated through  $7\alpha$ -hydroxylation of sterol precursors (predominately cholesterol itself) by cholesterol  $7\alpha$ -hydroxylase (CYP7A1) or one of two oxysterol  $7\alpha$ -hydroxylases (11).

Cholesterol metabolism in the brain is unique from other organs. Endothelial cells surrounding capillaries of the CNS are intimately associated with one another through tight junctions, or zona occludens, which form a protective impediment to solute diffusion known as the blood-brain barrier. The presence of the blood-brain barrier prevents interaction of cells within the CNS with circulating lipoproteins, mandating that 100% of the organ's cholesterol

demand be met by *de novo* synthesis. Likewise, the presence of the blood-brain barrier necessitates an alternative pathway for cholesterol excretion from the CNS. It was suggested early on that this pathway might involve hydroxylation of the cholesterol side chain and net efflux of a candidate, 27-hydroxycholesterol, from the brain was investigated; however, examination of arterio-venous differences in circulating oxysterols over the brain revealed the net excretion of a different molecule: 24(*S*)-hydroxycholesterol (12). The presence of high concentrations of this sterol in the brain relative to other tissues had previously earned 24-hydroxycholesterol the monicker ‘cerebrosterol’ in the 1950s (13), although the oxysterol’s importance to brain cholesterol metabolism and cognition were not apparent at that time. Conversion of cholesterol to 24-hydroxycholesterol facilitates cholesterol turnover from the brain by improving the sterol’s solubility, allowing the sterol to freely diffuse across the blood-brain barrier down a concentration gradient. In support of this pathway, 24-hydroxylation of cholesterol shortens the half-life of the molecule in the rat brain from 2-4 months to approximately 12 hours (14). Following efflux from the CNS, 24-hydroxycholesterol is transported to the liver via lipoprotein particles where the oxysterol is converted to bile acids (15).

Lutjohann and colleagues hypothesized that a dedicated enzyme activity responsible for the conversion of cholesterol to 24-hydroxycholesterol might exist in the brain (12). The enzyme that catalyzes this reaction was cloned from a

mouse liver cDNA library by Lund et al. in the mid-1990s (16). The newly characterized cholesterol 24-hydroxylase represented a previously undocumented and somewhat atypical subfamily of cytochrome P450s (P450s), termed CYP46. Like other P450s, 24-hydroxylase shares a common P450 fold, a heme prosthetic group, interaction with a redox partner and dependence on molecular oxygen (17, 18). 24-hydroxylase also requires NADPH as a cofactor for its catalytic activity (17). In contrast to the other P450s, the enzyme contains a proline-rich segment at the extreme carboxy-terminus, which is being investigated as a candidate protein interaction motif. Levels of the enzyme accumulate in the mouse and human brain with age, consistent with increasing concentrations of 24-hydroxycholesterol in the same organs over time (16). Interestingly, *CYP46A1* (the gene encoding 24-hydroxylase) and the associated protein product are highly conserved among vertebrate species and orthologues can be identified as far back in the evolutionary tree as echinoderms (D.W. Russell, personal communication).

The above findings suggested a crucial role for cholesterol 24-hydroxylase in brain lipid metabolism. To investigate this hypothesis, a strain of mice was engineered to lack expression of the enzyme (19). The mutant animals were produced through standard gene targeting methods, with a vector directed at exon 1 of *Cyp46a1*. The introduced mutation fully ablates cholesterol 24-hydroxylase cDNA and protein production. In its place, a heterologous DNA encoding a tau- $\beta$ -galactosidase (LacZ) fusion protein was introduced, such that reporter gene

expression is under control of the endogenous *CYP46A1* regulatory elements.  $\beta$ -galactosidase reporter activity was used to examine the expression pattern of 24-hydroxylase. Lund et al. demonstrated that 24-hydroxylase has a restricted pattern of expression, limited to particular sub-classes of neurons of the CNS. These findings were consistent with the group's previously reported *in situ* mRNA hybridization results (16).

Upon gross examination, 24-hydroxylase mutant mice appear indistinguishable from wild-type controls. With the singular exception of a 60-80% reduction in levels of serum 24-hydroxycholesterol, sterol levels and bile acid production are normal. Offspring from heterozygous matings exhibit a normal Mendelian pattern of inheritance of the mutant allele and the lifespan of 24-hydroxylase deficient mice is normal. There are no alterations overall in body weight or mass of individual organs. Mutant mice exhibit no outward abnormalities in mating, grooming, feeding, or circadian behaviors (personal observation); however, 24-hydroxylase deficient mice exhibit a 40-50% reduction in cholesterol synthesis specifically in the brain (19). This phenomenon occurs as a result of the inability of unmodified cholesterol to be removed across the blood-brain barrier, which leads to negative feedback on the cholesterol biosynthetic pathway. As a consequence, absolute cholesterol levels in the brains of these animals are normal, as is brain morphology down to the electron microscopic level (20).

Interestingly, absence of cholesterol 24-hydroxylase and the concomitant reduction in brain cholesterol turnover have a profound effect on cognitive function (20). 24-hydroxylase knockout (KO) mice show an inability to improve at tasks requiring spatial, contextual or motor learning. Additionally, induction of long-term potentiation (LTP, a proposed molecular correlate to learning and memory) is impaired at the synapses between pyramidal neurons of regions CA3 and CA1 in the hippocampus. Other aspects of synaptic transmission and plasticity, including spontaneous synaptic vesicle release (as determined by quantification of miniature synaptic currents) and long-term depression, are normal (20).

The 24-hydroxylase KO mice have two distinct, though related, metabolic abnormalities: 1) reduction in levels of 24(*S*)-hydroxycholesterol in the brain and plasma resulting from loss of cholesterol 24-hydroxylase activity, and 2) reduction in brain cholesterol synthesis due to feedback by accumulating cholesterol on the mevalonate pathway. Kotti *et al.* used the LTP paradigm to independently investigate the role of each of these metabolic defects on the cognitive abnormalities exhibited by 24-hydroxylase null mice. Oxysterols, including 24-hydroxycholesterol, have been shown to be potent activators of the liver X receptors (LXR $\alpha$  and LXR $\beta$ ), ligand-activated transcription factors of the nuclear hormone receptor superfamily (21). LXRs form obligate heterodimers with the retinoid X receptor (RXR) and upon ligand binding have been shown to

activate expression of genes involved in lipid metabolism (22). In order to test whether loss of 24(*S*)-hydroxycholesterol signaling through LXR could explain the synaptic defects in the 24-hydroxylase KO mouse, Kotti et al. measured LTP in mice lacking LXR $\alpha$  and LXR $\beta$ . These mice exhibited normal induction and duration of LTP with respect to wild-type slices, indicating that this pathway is not responsible for the LTP deficit in 24-hydroxylase KO mice (20). Current evidence suggests that instead, the disruption of metabolite flux through the mevalonate pathway is responsible for the observed LTP phenotype. Exogenous administration of mevalonate or the isoprenol geranylgeraniol to hippocampal slices prior to LTP-inducing theta-burst stimulation is sufficient to restore potentiation to WT levels (20).

Despite the vital role cholesterol plays in normal cellular physiology, this molecule is most widely identified with an involvement in human pathology. Notably, high levels of circulating cholesterol transported as LDL are associated with an increased risk of coronary artery disease and myocardial infarction (23), hence the common epithet “bad” cholesterol. In addition to numerous environmental and dietary factors that can affect lipid homeostasis, a variety of genetic disorders have been described that arise from defects in cholesterol metabolism and lead to severe disease in humans (24). The most prominent among these is familial hypercholesterolemia (FH) resulting from loss of LDL receptor function. Patients with FH have plasma LDL levels that are several

times greater than normal. They develop xanthomatous lesions of the skin and tendons and coronary artery disease at a very early age (25). Myocardial infarction may occur before the age of 2 years and homozygous inheritance of FH mutations usually result in death by early adulthood.

Altered brain cholesterol metabolism is also centrally involved in the etiology of numerous neuropathologies. Mutations in the cholesterol transport proteins NPC1 or NPC2 produce an autosomal-recessive lipid storage disorder known as Neiman-Pick type C disease (NPC). NPC is characterized by accumulation of a variety of lipids (including cholesterol) in the endosomal compartment of cells of the liver, spleen and brain (26). The disease is marked by progressive neurodegeneration, particularly affecting the thalamus and Purkinje cells of the cerebellum. The course of disease is variable among patients, but common symptoms include ataxia, speech impairments and dementia. Ultimately death ensues, before the age of 15 in some forms of the disease. NPC1 and NPC2 are sterol binding proteins that appear to act along the same intracellular pathway to transfer cholesterol out of the lysosomal compartment (27). Mouse models of NPC recapitulate major features of the disease, particularly endosomal lipid accumulation, demyelination and neurodegeneration, with death occurring between 11 and 12 weeks of age (28). Published findings from animal models strongly suggest that the pathology of the disease is dependent on accumulation of cholesterol rather than other lipids (28, 29).

To date, there have been no reported cases of human cholesterol 24-hydroxylase deficiency. There are suggestions, however, that polymorphisms in the CYP46A1 gene may be associated with impairment in synaptic function and neurodegenerative disease (30). Since 2002, at least 23 studies have been published that attempt to explore the relationship between one or more polymorphisms in *CYP46A1* and Alzheimer's disease (summarized at [www.alzforum.org](http://www.alzforum.org)); however, there is no consensus among these studies, as half of them report effects of the investigated polymorphism on AD progression and the remaining half demonstrate negative findings. Likewise, it has been purported that plasma levels of 24-hydroxycholesterol may be altered in patients with neurodegenerative disease. According to Lutjohann et al., plasma levels of 24-hydroxycholesterol vary inversely with the severity of disease, such that elevated plasma levels of this sterol may be used as an early marker of neurodegeneration (31); however, plasma concentration of 24-hydroxycholesterol may be dependant on the rate of hepatic clearance and has been demonstrated to vary widely, particularly with age and LDL cholesterol levels (32, 33).

Multiple disorders of lipid metabolism are associated with polymorphisms and mutations in the gene encoding for apolipoprotein E (ApoE), a 37 kDa glycoprotein found on the surface of chylomicron remnants,  $\beta$ VLDL and some HDL particles, conferring an ability on these particles to interact with LDL- and ApoE receptors (34). ApoE is the predominate apolipoprotein of the central

nervous system, where it resides on lipoprotein particles that resemble HDL. These lipoproteins are thought to be produced by astrocytes for distribution of lipids among the cells of the CNS, particularly to distal neurites and sites of injury repair (35). As such, neurons express a variety of receptors that are capable of mediating the internalization of ApoE-associated lipoproteins, including the LDL and VLDL receptors, LDL receptor-related protein (LRP), the ApoE receptor 2 (ApoER2) and megalin (26). In humans, ApoE exists in three isoforms (ApoE2, 3 and 4 encoded by alleles  $\epsilon$ 2,  $\epsilon$ 3 and  $\epsilon$ 4) that differ only in amino acid constitution at two sites (36). ApoE  $\epsilon$ 3 is most frequent allele among many ethnic populations, with an allele frequency of about 0.74. ApoE2 has been shown to interact with low affinity to the LDL receptor, making internalization of ApoE2-containing particles inefficient. Failure to clear these particles leads to a disorder in E2 homozygotes known as dysbetalipoproteinemia, where levels of  $\beta$ VLDL and chylomicron remnants in the circulation are high, while LDL and total cholesterol levels remain at or below normal (37). Patients with this genotype are also at increased risk for development of type III hyperlipoproteinemia, a disorder characterized by high circulating levels of VLDL cholesterol, hypertriglyceridemia and premature cardiovascular disease (38).

It was discovered in the mid-1980s that large amounts of ApoE are synthesized at sites of peripheral and optic nerve injury (39, 40). This finding led to the conclusion that ApoE may be required for storage and delivery of

cholesterol to neuronal membranes during injury repair. ApoE4 is thought to be less effective than ApoE2 or E3 in this process. There is evidence that the neuroprotective effects of ApoE are mediated through signaling properties intrinsic to the apolipoprotein receptors (specifically ApoER2), rather than as a direct result of lipid delivery (41). Reelin, a protein first identified in mutant mouse models, binds to both ApoER2 and VLDLR, initiating a downstream signaling cascade dependent on Disabled (DAB-1) (42). Loss of this signaling pathway results in severe neurodevelopmental and behavioral phenotypes in both mice and humans (43).

One of the most intensively investigated yet elusive neuropathologies associated with ApoE is the link between inheritance of ApoE  $\epsilon$ 4 allele and development of late-onset Alzheimer's disease (AD)(44). AD is a progressive, fatal neurodegenerative disorder that is the leading cause of dementia among the elderly. ApoE  $\epsilon$ 4 is associated with AD in a dose-dependent manner, with  $\epsilon$ 4/ $\epsilon$ 4 carriers being at highest risk and having earlier and more rapid development of symptoms than any other ApoE genotype (45, 46). The allele frequency of ApoE4 has been shown to be as high as 0.50 in patients with AD compared with 0.14 in the general population (44, 47). Strikingly, more than 80% of ApoE  $\epsilon$ 4 homozygotes will develop AD by the age of 80 (45, 48).

Alzheimer's disease was first described in 1907 by Alzheimer, a German physician who identified a devastating dementing disorder in a relatively young

patient named Auguste D. This subject was brought to a hospital in Frankfurt, Germany by her husband in 1901, at the age of 51 (49). At the time, she was exhibiting progressive behavioral abnormalities that began with paranoia and feelings of intense jealousy toward her husband. Auguste D. died in 1906 and her brain was examined histologically by Alzheimer, who reported findings of “intracellular fibrils” and “miliary foci” - now known as neurofibrillary tangles and amyloid plaques, respectively. Two years after Alzheimer’s report, a colleague named Perusini published his own findings on four similar cases, with case number 1 being the same Auguste D. At the time, Perusini recognized that the disease suffered by his young patients represented a form of “presenile disease” “recalling the main features of senile dementia” (49, 50). Thus, it was recognized that the dementia referred to as ‘Alzheimer’s disease’ existed in two forms, early-onset (pre-senile) and senile, that shared common presentation and histopathological features.

Major advances into the genetics of and molecular events thought to underlie AD began in the early 1980s (51). In 1984, Glenner published the sequence of amyloid- $\beta$  peptide ( $A\beta$ ), the major component of the extracellular and cerebrovascular amyloid deposits observed in the post-mortem brains of AD patients (52). In the same year, Glenner also published a report that proposed a relationship between AD and Down’s syndrome. The same  $A\beta$  peptide that had been found to comprise amyloid in AD was identified in the cerebrovascular

amyloid deposits of two individuals with Down's syndrome (53) a genetic disorder resulting from full or partial trisomy of chromosome 21. In the years surrounding these discoveries, there were multiple reports describing heritability of AD in families, some of which coincidentally demonstrated higher than normal incidence of Down's syndrome (54-56). Taken together, these findings suggested an AD susceptibility locus on chromosome 21, as was suggested by Glenner, who also proposed that the presence of A $\beta$  peptide might be used as a diagnostic screen for AD (53).

By the early 1990s, the gene encoding A $\beta$  peptide had been identified as amyloid precursor protein (APP) on chromosome 21 and genetic linkage had been used to identify mutations of this gene in families with early-onset, autosomal dominant forms of AD (57, 58). APP is a type I transmembrane protein with an as yet undetermined biological function. APP deficient mice are viable and exhibit relatively subtle growth and behavioral abnormalities, whereas mice lacking APP and two structurally related gene-family members, amyloid precursor-like proteins 1 (APLP1) and 2 (APLP2), do not survive to birth (59). APP interacts with the adaptor protein Fe65, and targeted deletion of Fe65 and other family members in mice yields a phenotype similar to the APP family member triple knockout (60). Fe65 has been shown to form a transcriptionally active complex with the intracellular domain of APP *in vitro* (60), but it is not yet clear what the functional relevance of this interaction is in the adult human brain.

Other reports suggest that the extracellular domain of APP is necessary for biological function (61).

Amyloid precursor protein is sequentially proteolytically processed to generate peptide fragments, among which is A $\beta$  (Figure 2). The first step in the APP proteolytic cascade occurs either at the cell surface or within endosomes and is carried out by  $\alpha$ - or  $\beta$ -secretases. Alpha-secretases are members of the ADAM (A Disintegrin And Metalloproteinase) family of zinc proteases that cleave the extracellular domain of APP within the A $\beta$  sequence (62). This cleavage destroys the A $\beta$  peptide, leading to production of non-amyloidogenic species. Conversely, proteolysis of the APP ecto-domain can occur through the action of  $\beta$ -secretase or BACE-1 (for  $\beta$ -site APP Cleavage Enzyme). BACE-1 is a type I transmembrane aspartyl protease that cleaves APP further from the membrane than does  $\alpha$ -secretase (63). Cleavage at this more distal site is responsible for generation of the amino-terminus of A $\beta$ .

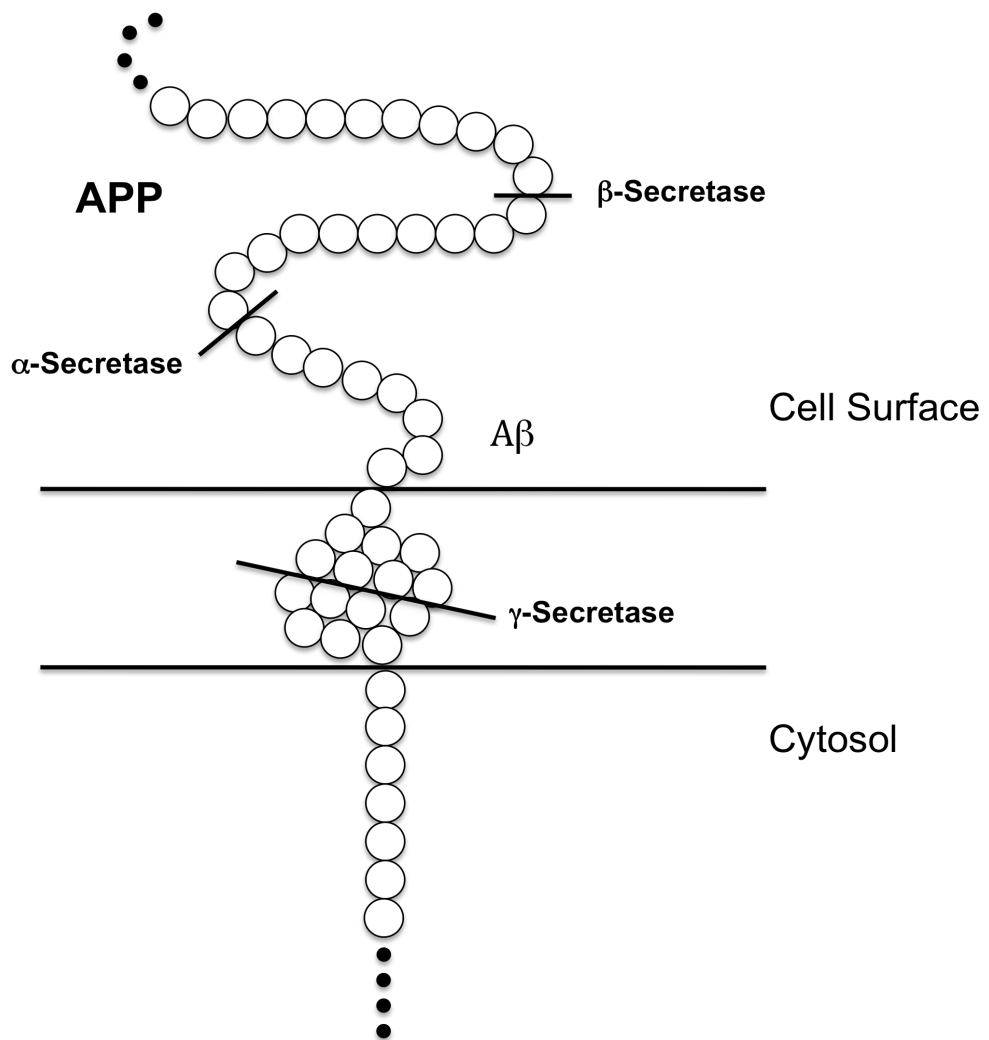


**Figure 2: Diagram of APP Processing.** APP is proteolytically processed by three enzyme activities termed  $\alpha$ ,  $\beta$  and  $\gamma$ -secretase. Cleavage by  $\gamma$ -secretase occurs within the membrane bilayer only subsequent to either  $\alpha$ - or  $\beta$ -secretase cleavage. Sequential processing at the  $\beta$ - and  $\gamma$ -sites yields  $A\beta$  peptides that vary between 39 and 43 amino acids in length. The longer species accumulate into characteristic amyloid plaques found in the brains of people with AD.

After cleavage by  $\alpha$ - or  $\beta$ -secretase, APP becomes a substrate for  $\gamma$ -secretase.  $\gamma$ -Secretase has been shown to comprise four proteins, Presenilin-1 or 2 (PSEN1/2), Nicastrin, APH-1 and PEN-2, which interact to yield a catalytically active complex (64). The presenilins are aspartyl proteases that constitute the enzymatic activity of the complex, whereas nicastrin is necessary for substrate recognition (64). The nature of the reaction carried out by  $\gamma$ -secretase is referred to as regulated intramembrane proteolysis (RIP), an evolutionarily conserved process by which single-pass transmembrane proteins are cleaved within their membrane-spanning regions (65). The acronym RIP was first coined in studies of the site-2 protease (S2P), a zinc metalloprotease responsible for processing sterol regulatory element binding proteins (SREBPs), which are involved in maintaining cellular cholesterol homeostasis. In the case of SREBP (and other transmembrane signaling proteins, such as Notch), the intracellular domain released by RIP is translocated to the nucleus, where the fragment functions as a transcriptional regulator (65). RIP cleavage of APP yields peptides ranging from 39- to 43 amino acids in length, with the longer peptides demonstrating greater propensity to aggregate into plaques. The most abundant among these fragments are  $A\beta_{40}$  and  $A\beta_{42}$ , with the value in subscript representing the number of amino acids in the peptide.

While a multitude of ideas regarding the etiology of AD have derived from these findings, the 'amyloid cascade' hypothesis became and remains the

predominate hypothesis driving AD research (66). According to this theory, the pathological events that precipitate cognitive decline in AD begin with abnormal or excessive processing of the amyloid precursor protein. The amyloidogenic products of proteolysis aggregate into plaques, causing a series of molecular changes that lead to synaptic malfunction, tau hyperphosphorylation/neurofibrillary tangle formation and ultimately neuron cell death. This pathway of events is supported by several lines of evidence, including the findings that 1) mutations in the APP gene are sufficient to cause AD, 2) that gene triplication of APP in Down's syndrome leads invariably to AD in the fourth or fifth decade of life, 3) that diffuse A $\beta$  deposits precede senile plaque formation (implying a precursor-product relationship), neurofibrillary tangles and neurodegeneration and 4) that A $\beta$  peptides have been shown to exhibit neurotoxic properties in vitro (66, 67). APP mutations were later shown to account for only a very small proportion of FAD cases (68), but the findings provided impetus to the scientific community to search for additional AD genes in the hope of gaining insight into the underlying cause of the disease.

It is now known that mutations in at least three genes are responsible for early-onset FAD in kindreds with multiple members affected over several generations ([www.alzforum.org](http://www.alzforum.org)). In addition to APP, mutations in *PSENI* (chromosome 14) and *PSEN2* (chromosome 1) have been identified. *PSENI* mutations were first reported in 1995 and account for the majority of early-onset

FAD cases (47, 69, 70). PSEN2 is structurally related to PSEN1, but mutations in this gene account for fewer FAD cases (47). The common feature among all early-onset AD mutations is believed to be a propensity for APP cleavage that yields longer, more amyloidogenic A $\beta$  species. Mutations in these three genes follow a fully penetrant, autosomal-dominant mode of inheritance and result in disease that begins before the age of 65. In affected individuals, the disease is aggressive and progresses more quickly than in cases of senile (or late-onset) AD; however, familial, early-onset cases only account for one out of every twenty AD cases (51). Most patients presenting with AD exhibit 'sporadic' development of the disease with onset after the age of 65. Although there is strong evidence for heritability of late-onset AD, no causative genes have been identified (51).

To date, there are no cures for AD and current therapies are at best modestly effective at delaying symptoms of cognitive decline (71). Investigations into new treatments center around the series of pathological events posited in the amyloid cascade hypothesis. These primarily include reducing plaque burden by inhibiting processing of APP to A $\beta$ , promoting alternative cleavage of APP by  $\alpha$ -secretase and accelerating clearance of A $\beta$  from amyloid plaques. Owing to a putative role for altered cholesterol metabolism in AD, the therapeutic potential of cholesterol-lowering statin drugs is being intensively investigated (72). The results of many large-scale studies (both retrospective and prospective) have been largely inconclusive; however, some data show that statins exert beneficial effects

that are both dependent on and independent of cholesterol lowering (73). In particular, during statin therapy, levels of intermediates in the cholesterol biosynthetic pathway are reduced as a direct consequence of HMG CoA reductase inhibition. Production of the isoprenoid compounds farnesyl and geranylgeranyl diphosphate is compromised. These compounds are used to modify (prenylate) small G-proteins of the ras superfamily. In the absence of prenylation, G-protein function is disrupted and one outcome is a decrease in the inflammatory response (73). As mentioned above, disruption of the flux of metabolites through the cholesterol biosynthetic pathway also appears to be the cause of the cognitive phenotype exhibited by 24-hydroxylase KO mice.

To further explore the consequences of alterations in cholesterol synthesis on the development of AD pathology, I designed a study using cholesterol 24-hydroxylase deficient mice as a model of chronic reduction of brain cholesterol synthesis. In some respects, cholesterol 24-hydroxylase KO mice represent a model of chronic CNS administration of HMG CoA reductase inhibitors (i.e., statins) in that they exhibit a marked reduction in brain cholesterol synthesis, albeit through a different mechanism. In humans, there remains uncertainty about the ability of statins to penetrate the blood-brain barrier and thereby mediate long-lasting changes in cholesterol synthesis. Defects in 24-hydroxylase KO mice are specific to brain and persist throughout life. Animals lacking 24-hydroxylase were crossed to double-transgenic mice expressing human APP and PSEN1 proteins

bearing mutations associated with early-onset AD (74). Pathological hallmarks associated with AD were examined in these animals over time. Tissues were harvested at three-month intervals between the ages of 3 and 15 months. I examined amyloid plaque accumulation in the hippocampus and cerebral cortex, two regions of the brain known to be affected in AD and known to express cholesterol 24-hydroxylase at high levels to determine if plaque deposition is affected by alterations in cholesterol synthesis. I also investigated changes in APP processing by quantifying levels of A $\beta_{40}$  and A $\beta_{42}$  peptides in soluble and insoluble (plaque) pools within these same brain regions. Additionally, I examined relative levels of proteins involved in AD and cholesterol metabolism by immunoblotting to look for changes in protein levels between 24-hydroxylase WT and KO mice. To determine if high levels of A $\beta$  peptides or amyloid plaques were capable of modulating lipid synthesis *in vivo*, rates of cholesterol and fatty acid synthesis were measured in aged AD animals. Finally, I designed a study to examine the effects of AD pathology on longevity in this mouse model. Together, the findings from these experiments provide insight into the interplay between cholesterol metabolism in the brain and AD. Additionally, this genetic model may be used to assess the value of statin therapy for patients with AD.

## MATERIALS AND METHODS

### I. Mouse Model

Mice lacking the enzyme cholesterol 24-hydroxylase (24-hydroxylase) were generated previously by targeting of the *Cyp46a1* gene through homologous recombination in mouse embryonic stem cells, to generate a null allele (19). The B6.Cg-Tg(APP<sup>swe</sup>, PSEN1E9)85Dbo/J (line 85) Alzheimer's disease (AD) model was obtained from Jackson Laboratories (stock number 005864; Bar Harbor, Maine). This mouse was generated by pronuclear co-injection of two individual linearized vectors, one encoding a human/mouse chimeric amyloid precursor protein (APP) harboring the Swedish (K670N/M671L) Alzheimer's disease mutations (75) and the other encoding a human Presenilin 1 (PS1) protein with deletion of exon 9, both driven by mouse prion promoters (74). AD mice were maintained in the hemizygous state. To produce the animals used in this study, 24-hydroxylase KO mice on a mixed 129S6/SvEv x C57BL/6J background were mated to B6C3F1/J AD descendants of line 85 that had been backcrossed to C57BL/6J for at least 8 generations (information obtained from Jackson Laboratories). Subsequently, 24-hydroxylase heterozygous/AD hemizygous (HET/AD) animals were crossed to 24-hydroxylase heterozygous animals to generate all possible genetic combinations and sexes of 24-hydroxylase and AD.

The genotypes of offspring were determined by PCR at weaning (between 3 and 5 weeks of age) and, for animals used in a given experiment, were confirmed following euthanasia. A 5 mm segment of tail was clipped and digested overnight at 55°C in 500  $\mu$ L tail digestion buffer (100 mM Tris-HCl pH 8.5, 5 mM EDTA, 0.2% SDS (w/v), 200 mM NaCl) containing 100 mg/mL proteinase K. Undigested material was removed by centrifugation in a microcentrifuge at 14,000 rpm for 5 minutes. DNA was precipitated by transfer of the resulting supernatants into new 1.5 mL microcentrifuge tubes containing 500  $\mu$ L 100% isopropanol. Samples were gently shaken at room temperature for about 30 minutes or until DNA precipitates became visible. The DNA was then pelleted by centrifugation at 14,000 rpm for 10 minutes. The supernatant was removed by inversion of the tubes onto absorbent paper and pellets were dissolved in 500  $\mu$ L TE buffer (10 mM Tris-HCl, 1 mM EDTA; pH 8.0). One  $\mu$ L of each DNA preparation was used per PCR reaction. PCR genotyping protocols for 24-hydroxylase and the line 85 AD transgenic mouse model are described by Lund et al. and Jankowsky et al., respectively (19, 74). PCR primers were purchased from Integrated DNA Technologies (Coralville, IA) and native *Taq* DNA Polymerase (Invitrogen; Carlsbad, CA) was used according to the manufacturer's instructions. PCR Nucleotide Mix was purchased from Roche Applied Science (Indianapolis, IN) and used at a final concentration of 200  $\mu$ M each dNTP. The 24-hydroxylase and APP/PSen1 PCR products were separated

on 2% and 1% agarose (w/v, Sigma-Aldrich; St. Louis, MO) gels, respectively. Agarose was prepared in 1x TBE (0.9 M Tris-borate, pH 8.0, 20 mM EDTA) and ethidium bromide was added to a final concentration of 1  $\mu\text{g}/\text{mL}$  to allow product visualization by UV transillumination. Gels were subjected to electrophoresis in a Sub-Cell GT horizontal electrophoresis chamber in 1x TBE using a PowerPac Basic power supply (Bio-Rad) at 100 V for up to 90 minutes.

## **II. Tissue Collection**

For amyloid plaque and A $\beta$  peptide quantification, male and female animals of all six possible genotypes were killed at 3, 6, 9, 12 and 15 months of age,  $\pm$  7 days ( $n \geq 5$  per group). Animals were sedated in a chamber containing isoflurane inhalation anesthetic, then deeply anaesthetized with an intraperitoneal injection of 5 mg/mL ketamine/0.5 mg/mL xylazine (400  $\mu\text{L}/10$  g body weight) diluted from stock solutions into physiological saline (0.85% NaCl (w/v)). The heads of sedated animals were immobilized in the prone position on a stereotactic frame using ear bars designed for small rodents. The skin and muscles were removed from the base of the skull and a midsagittal incision was extended down the spine beyond the upper thoracic region. The nose was secured toward the chest in order to stretch the back of the neck. A small hook made from the bent tip of a 23-gauge hypodermic needle was used to pull gently on the atlas

to reveal the cisterna magna. The dura covering the cisterna was punctured with a pulled microcapillary pipette connected through stiff, airtight Teflon tubing to a 100  $\mu$ L Hamilton GasTight™ syringe (Sigma-Aldrich). With this setup, gently pulling the syringe plunger draws CSF into the micropipette. After removal of CSF (routinely 2-15  $\mu$ L), animals were euthanized by lethal exposure to isofluorane. CSF was dispensed onto a small sheet of Parafilm and the volume was determined using a 10  $\mu$ L Drummond Dialamatic Microdispensor (Sigma-Aldrich). Finally, samples were drawn into the middle of glass microcapillary tubes. The ends of the tubes were heated with a miniature butane torch and were pinched shut with a small forceps to form an airtight seal. All samples were stored long-term at -80°C.

Following respiratory cessation, the abdominal cavities of experimental animals were opened and blood was drawn from the posterior vena cava using a 23-gauge needle attached to a 0.5 M EDTA-rinsed 1 mL syringe. Animals were decapitated and the brains were carefully removed, weighed and placed in a 60 mm tissue culture dish containing ice-cold 1x Hank's balanced salt solution without calcium, magnesium or phenol red (HBSS, Invitrogen; Carlsbad, CA). Subsequently, the liver was perfused through the hepatic portal vein with 3 mL ice-cold HBSS to remove the majority of blood. After perfusion, the liver was removed, weighed and wrapped in labeled aluminum foil for long-term storage at -80°C. Finally, under a dissecting microscope (Leica Wild MZ8, 12.5x

magnification), the intact brain was divided mid-sagittally into right and left halves. The left half was prepared for future histological examination by fixation overnight at 4°C in 4% PFA (w/v), cryoprotected for 24 hours in 30% sucrose (w/v) at 4°C, and stored long-term at -80°C until needed. From the remaining half, the cerebral cortex, hippocampus and cerebellum were isolated and placed in individual containers for storage at -80°C until needed. Finally, a piece of tail was cut to confirm the genotype. All tissues were frozen on dry ice immediately after dissection, until relocation to long-term storage at -80°C.

### **III. Plaque Visualization**

#### **a. Section Preparation**

Fixed hemi-brains from experimental animals were removed from -80°C storage and allowed to equilibrate to cutting temperature (-23°C ± 3°C) in the cryostat chamber for 30 minutes. Multiple 40 µm-thick coronal sections were made using a Microm HM550 OMVP cryostat (Richard Allen Scientific, now Thermo Scientific; Waltham, MA) specimen temperature, -18°C ± 3°C) from the genu of the corpus callosum through the caudal extent of the hippocampus. Sections were positioned successively onto one of six BondRite™ slides (Richard Allen Scientific), such that each slide contained every sixth section for a total of

18-21 sections per slide, 240  $\mu\text{m}$  apart in depth. Each slide was labeled only with the corresponding animal's unique identification number, which was assigned based on paternity and weaning order, but did not give any indication as to the sex, genotype or age of the animal at the time of euthanasia. Completed slides were left to dry overnight at room temperature. The next day, the slides were dried at 32°C on a slide warmer for 1 hour. After drying, slides were post-fixed in 4% PFA for 15 minutes, rinsed 5 times in ddH<sub>2</sub>O and subsequently incubated in 1% glycine (w/v) in PBS at room temperature for 1 hour. Following glycine treatment, slides were left overnight at room temperature to dry, then were stored at -80°C vertically in slide boxes which were wrapped with several layers of aluminum foil.

#### **b. Thioflavine S Staining**

Slides were removed from long-term storage and were allowed to warm to room temperature and dry before staining. Slides were rinsed in ddH<sub>2</sub>O then stained by immersion for 5 minutes in a solution of 1% thioflavine S (w/v, Sigma-Aldrich) in ddH<sub>2</sub>O. Slides were then moved to 70% ethanol for 5 minutes, rinsed 2 times in ddH<sub>2</sub>O and coverslips were mounted with Prolong Gold™ containing DAPI (Invitrogen), following the manufacturer's instructions. Mounting medium was allowed to cure overnight and coverslips were sealed at the edges with clear

nail polish. Thioflavine S exhibits green fluorescence (excitation, 430 nm; emission, 550 nm), with spectral characteristics resembling GFP and fluorescein. DAPI fluoresces strongly only when bound to DNA (excitation, 358 nm; emission, 461 nm) and was used to visualize cell nuclei.

### **c. Congo Red Staining**

Slides were removed from  $-80^{\circ}\text{C}$  storage as described above for Thioflavine S staining. Sections were stained with Congo Red and modified Mayer's hematoxylin (Amyloid Stain Kit, Richard Allen Scientific) to visualize amyloid plaque and cellular nuclei, respectively. Congo Red interacts with the  $\beta$ -pleated sheet structure of amyloid, dyeing the plaques red, thereby allowing visualization. The dye also exhibits an apple-green birefringence when viewed under polarized light. Hematoxylin stains nuclei dark blue. Congo Red working solution was prepared by adding 10 drops of the provided sodium hydroxide solution to 50 mL of Congo Red solution. Slides were stained in Congo Red working solution for 20 minutes at room temperature, rinsed for 1 minute with ddH<sub>2</sub>O and then were stained for 5 minutes in the provided modified Mayer's hematoxylin solution. Following hematoxylin staining, slides were immersed in bluing solution for one minute, rinsed with ddH<sub>2</sub>O and dehydrated through graded alcohols to xylene as per the manufacturer's instructions. Coverslips were

mounted using Mounting Medium from Richard-Allen Scientific and allowed to cure at room temperature overnight before imaging.

#### **IV. Plaque Quantification**

##### **a. Pilot Study**

An unbiased stereological approach was taken to characterize plaque accumulation in WT/AD and KO/AD mice. Experimental and sampling parameters were developed based on methods described by Mouton (76). A pilot study was conducted to determine the sampling frequency necessary to provide accurate results and sufficient power to perform statistical analyses. One slide from each of six 9-month old male AD mice (three WT and three KO) was chosen at random according to numbers produced by Research Randomizer, an internet-based random number generator (<http://www.randomizer.org/form.htm>; 1 unsorted set of 500 non-unique numbers ranging from 1-6). Selected slides were stained with Thioflavine S according to the protocol described above. Sections were viewed using an Olympus BX51WI microscope and imaged on a Dell computer monitor via FireWire™ connection to a top-mounted MicroFire™ digital, color CCD camera. Stereo Investigator (MBF Bioscience; Williston, VT) software version 6.0 was used for all stereological measurements and calculations.

An individual Stereo Investigator file containing all pertinent data was produced for each slide and results were also exported to Microsoft Excel for statistical analyses.

Viewing slides under the 4x objective with the DAPI filter, the Stereo Investigator contour feature was used to draw outlines of the cerebral cortex and hippocampus (if applicable) for every section on each slide. A separate contour label was used to distinguish cerebral cortical measurements from those of the hippocampus. The software calculated the area within the contours, and therefore, the area of the outlined structures. Once contours were drawn, objective strength was increased to 20x and the fluorescence filter was adjusted to visualize Thioflavine S-stained plaques. A computer-simulated stereological probe known as the Cavalieri point counting grid was generated to appear on the computer screen over the sections of interest. Grid points were programmed to appear uniformly every 5  $\mu\text{m}$  and colored near-black to blend in with the tissue background. Grid points overlaying fluorescent green plaques were easily identified by the observer and labeled using features inherent to the Stereo Investigator software. Plaques within the cerebral cortex were labeled with a different marker from those in the hippocampus. Labeled grid points were tallied for each tissue section and the area of plaque coverage estimated based on the number of grid points marked (76).

To compare results within and among experimental animals, data were converted to a fraction equaled to the area represented by plaque (as determined by the number of grid points labeled) divided by the total surface area of the region of interest (the area within the contour). Plaque fractions were displayed graphically using Prism (GraphPad Software; La Jolla, CA). From the results of the pilot study, it was demonstrated that plaque load would need to be measured in three sections from each slide to maximize sampling efficiency, while still achieving the desired statistical power (77).

#### **b. Thioflavine S v. Congo Red**

The pilot study also revealed uncontrollable variation in background signal on slides stained with Thioflavine S. In order to account for this variation, background fluorescence was standardized by adjusting the duration of fluorescence image capture; however, even slight alterations in capture time yielded significant changes in the apparent size of plaques, making direct comparisons between slides impossible. Therefore, Congo Red, a colorimetric amyloid stain was utilized as a dependable method of visualizing plaques in brightfield microscope images. This method was employed for all plaque quantification subsequent to the Pilot Study. All slides from selected age groups were stained simultaneously in staining dishes capable of holding up to 50 slides.

Slides were processed according to the protocol described above for Congo Red staining.

### **c. Plaque Quantification in Study Animals**

One slide from each study animal was selected randomly and stained with Congo Red, as described above. Results of the pilot study demonstrated that amyloid plaques were distributed evenly throughout the rostral-caudal extent of the cerebral cortex, thus three sections spaced 720  $\mu\text{m}$  apart and containing both cerebral cortex and hippocampus were chosen. Slides were labeled only with the unique animal number and contained no identifying marks or anatomical abnormalities that could be used to distinguish one sex or genotype from another. Slide labels were decoded only following completion of each age group in the study to avoid the introduction of bias.

Plaque load was determined using the counting method described in the Pilot Study and results were exported to Microsoft Excel and Prism for statistical analyses. Student's t-test was conducted within Prism to assess differences between groups. After completion of the study, a linear regression was calculated for all experimental groups, demonstrating positive linear correlation between plaque fraction and age in all AD sex/genotype combinations in cerebral cortex and hippocampus.

## V. A $\beta$ Peptide Quantification

### a. Tissue Homogenization

Brain tissues were thawed on ice and each sample was weighed to the nearest milligram (mg). Tissues were homogenized in ice-cold radioimmunoprecipitation assay (RIPA) buffer (150 mM NaCl, 1.0% NP-40 (w/v) 0.5% sodium deoxycholate (w/v), 0.1% SDS (w/v) and 50 mM Tris-HCl, pH 8.0) containing Complete<sup>TM</sup> EDTA-free protease inhibitor cocktail (Roche Applied Sciences; Indianapolis, IN) using a miniature 1-2 mL Dounce homogenizer (15 strokes, tight pestle), as follows:

Cerebral cortex: 1000  $\mu$ L RIPA; Q.S. to 1500  $\mu$ L after ultracentrifugation

Hippocampus: 400  $\mu$ L RIPA; Q.S. to 500  $\mu$ L after ultracentrifugation

RIPA homogenates were transferred to labeled thick-walled polycarbonate ultracentrifuge tubes and subjected to ultracentrifugation at 100,000 x g (53,000 rpm in a TLA-100.2 rotor) in a Beckman Optima TLX ultracentrifuge (Beckman Coulter; Fullerton, CA) for one hour at 4°C. The resulting supernatants were transferred to 1.5 mL microcentrifuge tubes and final volumes adjusted to those listed above. Pellets were resuspended in ice-cold 70% (v/v) formic acid by trituration using a P200 Pipetman (Gibson; Middleton, WI) with a 200  $\mu$ L tip (20 triturations), as follows:

Cerebral cortical pellets: 400  $\mu$ L; Q.S. to 500  $\mu$ L after ultracentrifugation

Hippocampal pellets: 100  $\mu$ L; Q.S. to 150  $\mu$ L after ultracentrifugation

Formic acid homogenates were ultracentrifuged for 80 minutes at 4°C and 100,000 x g as described for RIPA homogenates above. Immediately after centrifugation, cleared formic acid supernatants were removed from the centrifuge tubes using 200  $\mu$ L gel-loading Pipetman tips, taking care not to disturb the cloudy surface film or pellet. Supernatants were transferred to 1.5 mL microcentrifuge tubes and final volumes adjusted as described above. RIPA and formic acid homogenates were stored at -80°C until needed for A $\beta$  quantification.

#### **b. Protein Assay**

Protein levels in RIPA homogenates were determined using the Pierce (Pierce Biotechnology; Rockford, IL) BCA Assay kit, following the manufacturer's instructions. Briefly, 200  $\mu$ L of BCA working reagent was mixed with 25  $\mu$ L of sample (in duplicate) in a 96-well plate. Color was allowed to develop for 15-20 minutes at 37°C or 1-2 hours at room temperature and the absorbances of the samples were read at 570 nM using an Opsys MR microplate reader with Revelation Quicklink software (Dynex Technologies; Chantilly, VA). Absorbance of bovine serum albumin (BSA) protein standards diluted in RIPA +

protease inhibitors was plotted against concentration using Microsoft Excel (XY scatter plot with absorbance on the x-axis and concentration on the y-axis) and the standard curve was fit with a second-order polynomial trendline. Microsoft Excel 2007 software was used to calculate the equation of the trendline, from which sample concentrations were determined.

### **c. Quantitative ELISA**

A $\beta_{40}$  and A $\beta_{42}$  peptide levels in the cerebral cortex and hippocampus of study animals were determined by quantitative ELISA. The ELISA protocol used in this study was developed based on published protocols (78). Anti-amyloid beta (1-16) clone 6E10 (EMD Bioscience; Gibbstown, NJ and Covance; Princeton, NJ) was diluted 1:100 into bicarbonate coating buffer (0.1 M NaHCO<sub>3</sub>, 0.1 M Na<sub>2</sub>CO<sub>3</sub> pH 9.6). Reacti-Bind<sup>TM</sup> 96-Well ELISA plates (Pierce Biotechnology) were coated with 100  $\mu$ L/well of the 6E10 antibody dilution overnight at 4°C with gentle rotation. The following morning, plates were washed twice with 200  $\mu$ L/well of phosphate-buffered saline containing 0.05% (v/v) Tween 20 (PBST) and were blocked for 1 hour with 125  $\mu$ L/well Superblock<sup>TM</sup> buffer with Tween 20 (Pierce Biotechnology) at room temperature. Following blocking, plates were washed one time with 200  $\mu$ L/well PBST and stored at 4°C in an airtight container with 200  $\mu$ L PBST in each well.

As needed, coated assay plates were removed from 4°C storage and the storage solution was removed. A $\beta$  peptide standards and tissue homogenates were diluted to a range compatible with the assay and assayed in duplicate. Up to four different dilutions of each sample were included per plate in order to obtain at least two dilutions within the linear range of the assay. RIPA homogenates were assayed undiluted or diluted as needed with RIPA buffer containing protease inhibitors. Peptide standards were prepared in the same buffer. Formic acid homogenates were neutralized by adding 19 volumes of 1 M Tris base (pH unadjusted) and then diluted 2-40 fold with ddH<sub>2</sub>O. The presence of high concentrations of Tris in the samples was found to interfere with the assay, reducing sensitivity approximately 5-fold. Peptide standards for formic acid homogenates were prepared in neutralized formic acid that had been diluted with water to the same extent as the most concentrated sample. Subsequent dilutions of samples and standards were made in this buffer such that Tris base and formic acid concentrations remained constant in all wells. For samples in RIPA buffer, the assay standards were diluted serially from 4 ng/mL, and for formic acid samples, standards were diluted from 20 ng/mL.

100  $\mu$ L of each dilution was loaded per well and peptides were captured for 24 hours at 4°C with gentle rotation. After capture, plates were washed 3 times with 200  $\mu$ L/well PBST and 1 time in PBS + 0.5% Tween 20 (Surfact-Amps 20; Pierce Biotechnology) with 5 minutes of vigorous shaking during the

final wash. Following washing, captured peptides were detected with a primary rabbit polyclonal antibody specific for either A $\beta$ <sub>40</sub> or A $\beta$ <sub>42</sub> (PC149 or PC150, respectively; Calbiochem, now EMD Bioscience; Gibbstown, NJ). Primary antibodies were diluted to 0.5  $\mu$ g/mL in Starting Block<sup>TM</sup> blocking buffer with Tween 20 (Pierce Biotechnology) and 100  $\mu$ L of the dilution was added per well. Plates were incubated overnight at 4°C with gentle rotation.

On the final day, ELISA plates were removed from 4°C and washed as described above following the capture step. Mouse anti-rabbit horseradish peroxidase (HRP)-conjugated secondary antibody was diluted 1:2000 in Starting Block<sup>TM</sup> buffer with Tween 20 and 100  $\mu$ L was added to each well of the plate. Plates were covered with aluminum foil and incubated for 1 hour at room temperature with gentle rotation. Plates were washed as described above and dried by inversion onto absorbent paper with firm tapping. 100  $\mu$ L/well of ABTS HRP substrate solution (1-Step ABTS; Pierce Biotechnology) was added. Plates were allowed to develop at room temperature until the color in any of the wells reached dark green (usually 15-20 minutes). At this point, absorbance of the reaction product was measured at 405 nm using a Synergy 4 microplate reader run by Gen 5 software (BioTek; Winooski, VT). Data were exported to Microsoft Excel, which was used to prepare a standard curve (XY scatter plot with absorbance on the x-axis and concentration on the y-axis) and a linear trendline

was fit to the points on the curve. The equation of the trendline was calculated in Excel and used to determine the concentration of peptide in each sample.

## **VI. *In Vivo* Cholesterol Biosynthesis**

Rates of cholesterol biosynthesis in tissues of live animals were determined by measuring the incorporation of tritiated water ( $[^3\text{H}]\text{H}_2\text{O}$ ) into cholesterol over a fixed period of time (79). A series of studies was conducted to determine the effects of loss of 24-hydroxylase or advanced stage of plaque accumulation on rates of cholesterol biosynthesis in the whole brain and in specific brain sub-regions in mice. To determine 24-hydroxylase gene dosage effects on brain cholesterol synthesis, male and female mice ( $n \geq 5$  per group) ranging from 10-16 weeks of age were studied. Female mice between the ages of 11 and 14 months ( $n = 10$  per group) were used to examine effects of amyloid plaque and high  $\text{A}\beta$  peptide levels on cholesterol synthesis. By this age, both WT/AD and KO/AD male and female mice have abundant plaques in cerebral cortex and hippocampus with plaque burden being higher in females.

Experimental animals were group-housed through the morning of the experiment. Each animal was injected intraperitoneally with 50 mCi  $[^3\text{H}]\text{H}_2\text{O}$  and transferred to an isolated box inside a fume hood. Exactly one hour after injection, animals were euthanized by lethal isofluorane exposure. Blood was

removed from the posterior vena cava using a 23-gauge needle attached to an 0.5M EDTA-rinsed 1 mL syringe and thereafter transferred to a 1.5 mL blood collection tube (Sarstedt; Germany). Tissues were dissected, weighed to the nearest milligram and saponified in alcoholic potassium hydroxide at 65°C. Cholesterol was isolated following digitonin precipitation and petroleum ether extraction using a protocol derived from Jeske and Dietschy (80). Following cholesterol isolation, the remaining aqueous layer was acidified with HCl and fatty acids were extracted into hexane. Isolated cholesterol and fatty acid samples were dried in glass scintillation vials and dissolved in 1 mL methanol. 15 mL of 3a70B Complete Counting Cocktail scintillation fluid (Research Products International; Mt. Prospect, IL) was added. Samples were counted for 5 minutes each in a Beckman LS6500 Multi-Purpose scintillation counter. The specific activity of injected water was determined from analysis of blood samples, allowing the rate of incorporation of water into cholesterol and fatty acids to be calculated. Results were represented graphically using Prism, and Student's t-test was performed to assess differences between experimental groups.

## **VII. Analysis of Proteins Related to Cholesterol Metabolism and Alzheimer's Disease**

The amounts of several proteins related to cholesterol metabolism and Alzheimer's disease were assessed by immunoblotting. Brain homogenates were prepared from female mice aged 11-13 months (n = 3 per genotype). Animals were euthanized with isoflurane and brains were removed. Each brain was weighed then divided in half mid-sagittally. One half of the brain was fixed in 4% PFA (w/v) and cryoprotected in 30% sucrose (w/v) as described above in "Preparation of Brain Tissue for Plaque Counting". The remaining half was homogenized in 1 mL ice-cold TA buffer (2 mM CaCl<sub>2</sub>, 10% sucrose (w/v) and 50 mM Tris-acetate, pH 7.4) containing Complete<sup>TM</sup> EDTA-free protease inhibitor cocktail using a 2 mL Dounce homogenizer (20 strokes, tight pestle). Insoluble material was removed by centrifugation for 15 minutes at 14,000 rpm and 4°C in a microcentrifuge. Protein concentrations of cleared homogenates were determined using the Pierce BCA assay kit. Equal amounts (0.3 mg) of protein from each sample within a genotype were pooled and samples were diluted with TA buffer to a protein concentration of 2 mg/mL. Protein pools were then mixed with an equal volume of 2x Laemmli sample buffer (4% (w/v) SDS, 50% (v/v) glycerol, 0.02% (w/v) bromophenol blue, 125 mM Tris-HCl, pH 6.8;

Bio-Rad) containing 10% (v/v)  $\beta$ -mercaptoethanol followed by heating in a block for 10 minutes at 95°C.

Polyacrylamide gels were prepared according to recipes published in Molecular Cloning: A Laboratory Manual (81). Brain homogenate pools were loaded into wells of a 10% SDS-polyacrylamide gel and electrophoresed at 60-120 V in a Hoeffer SE260 mini-vertical electrophoresis unit (GE Healthcare; Pittsburgh, PA) until the dye front approached the bottom of the gel. Precision Plus<sup>TM</sup> All Blue protein standards (Bio-Rad) were loaded adjacent to samples to track the location and separation of proteins with molecular weights ranging between 15 and 250 kD.

Following transfer cell (Bio-Rad) powered by a PowerPac HC power supply (Bio-Rad). Polyacrylamide gels were equilibrated in 2 changes of Towbin transfer buffer (192 mM glycine, 25 mM Tris base, 10% (v/v) methanol, pH unadjusted) for 10 minutes each prior to transfer. PVDF membranes were hydrated according to the manufacturer's instructions and equilibrated for at least 5 minutes in transfer buffer. Extra-thick filter papers (three per gel, cut to size) were saturated with transfer buffer and transfer stacks were assembled as follows (from anode to cathode, with air bubbles being removed after each step): two sheets of extra-thick filter paper, PVDF membrane, gel, final sheet of filter paper. The cathode plate of the SD unit was placed firmly on top of the gel stack(s) and the safety cover was replaced. The PowerPac was programmed to conduct the

transfer for 30 minutes at a constant current of 5 mA per cm<sup>2</sup> of gel area and not to exceed a 25 V potential.

Following transfer, gel stacks were disassembled and the locations of protein standards on the membrane were marked with a solvent-resistant ink marker. Unoccupied sites were blocked using a solution of 5% non-fat dry milk (w/v) in PBST at room temperature for a minimum of 1 hour or overnight at 4°C. Following blocking, membranes were rinsed in PBST several times to remove residual milk and then probed overnight at 4°C with primary antibody diluted in PBST containing 1% (w/v) BSA. The next morning, membranes were washed 4 times in PBST for 5 minutes each, then incubated for 1 hour at room temperature with an HRP-conjugated secondary antibody diluted 1:10,000 into PBST containing 1% BSA (w/v). Membranes were washed again in 4 changes of PBST for 5 minutes each and incubated in 2 mL each of a working dilution of SuperSignal West Pico chemiluminescent HRP substrate (Pierce Biotechnology) for 5 minutes. In a darkroom, blots were exposed to HyBlot CL film (Denville Scientific; Metuchen NJ) for the duration necessary to obtain signals of the desired intensity.

For reprobing, antibodies were stripped from membranes using guanidine buffer (6 M guanidine HCl, 62.5 mM Tris-HCl, pH 6.8) with 100 mM  $\beta$ -mercaptoethanol added just prior to use. Stripping was performed for 30 minutes at room temperature then the buffer was washed off thoroughly with PBST.

Membranes were blocked again in PBST with 5% (w/v) non-fat dry milk prior to probing with new antibodies using the method described above.

**Description of antibodies used:**

- Mouse monoclonal against 24-hydroxylase clone 1A7 (82) used as neat monoclonal supernatant supplemented with Tween 20 to 0.05% (v/v)
- Mouse monoclonal against APP clone 1G6 (Covance; catalog number SIG-39180) diluted 1:5,000
- Mouse monoclonal against glial fibrillary acidic protein (GFAP) clone G-A-5 (Calbiochem; catalog number IF03L) used at 0.2  $\mu\text{g}/\text{mL}$
- Mouse monoclonal against Tau clone Tau46 (Covance; catalog number SIG-39423) used at 0.2  $\mu\text{g}/\text{mL}$
- Mouse monoclonal against  $\alpha$ -tubulin clone DM1A (Abcam; catalog number ab7291) diluted 1:10,000

**VIII. Survival Study**

Mice were committed to this study at the time of weaning ( $n \geq 12$  for all genotypes and sexes). Animals were housed in same-sex groups of between 2 and

4 and were not used for other purposes, including mating. Animals were identified by ear markings corresponding to unique animal numbers. Dead animals were removed from the colony and genotypes confirmed. Data were plotted and survival curves generated using Prism software.

## RESULTS

### I. Plaque Accumulation in AD Mice.

Alzheimer's disease is characterized by two histopathological lesions in the brain, neurofibrillary tangles and amyloid plaques. Amyloid plaques are extracellular deposits of  $A\beta_{42}$ , a peptide product of amyloid precursor protein (APP) proteolysis. It is believed that accumulation of these amyloidogenic  $A\beta_{42}$  peptides in AD leads to plaque formation, synaptic dysfunction and neurodegeneration. Most therapeutic approaches under investigation are aimed at preventing cerebral  $A\beta_{42}$  aggregation or promoting clearance of amyloid plaques from the brain. Several lines of transgenic mice have been engineered to accumulate  $A\beta_{42}$ -containing amyloid plaques in specific brain regions involved in AD. These mice have been utilized to study the ability of genetic manipulations and therapeutic agents to modify plaque accumulation and clearance. To assess whether or not AD mice lacking cholesterol 24-hydroxylase (24-hydroxylase) would exhibit amyloid plaque development, brain tissues from 9-month old male AD mice were examined. Tissue sections were stained with thioflavine S for plaque visualization and DAPI to identify cellular nuclei. AD mice with wild-type levels of 24-hydroxylase (WT/AD) exhibited abundant plaques in the cerebral cortex and hippocampus (Figure 3). 24-hydroxylase

deficient AD mice (KO/AD) of the same age also demonstrated advanced plaque accumulation. In contrast, 24-hydroxylase deficient mice lacking the AD transgenes (KO), as well as their non-transgenic 24-hydroxylase wild-type (WT) littermates did not exhibit plaque accumulation, even in very old age (Figure 1, and data not shown).

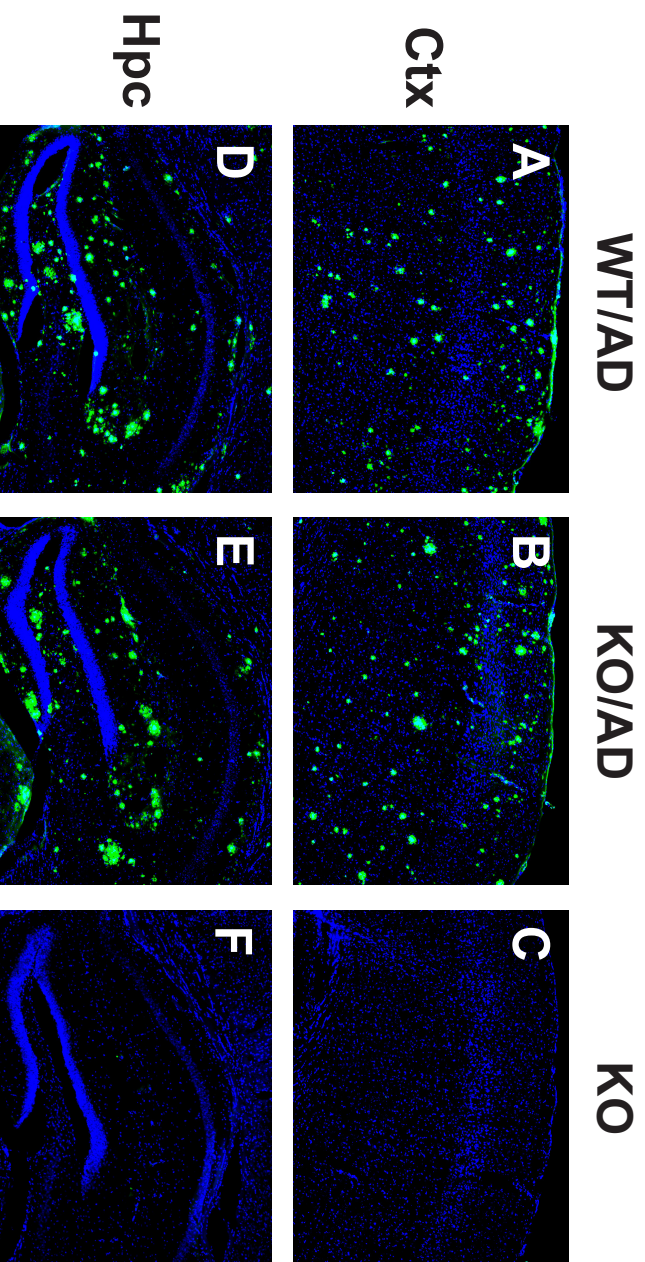


**Figure 3: Thioflavin S staining of amyloid plaque in 24-hydroxylase WT and KO cerebral cortex and hippocampus.** Cerebral cortical (Ctx) and hippocampal (Hpc) sections from 9-month-old male mice of the indicated 24-hydroxylase/AD genotypes were stained with thioflavine S and DAPI to visualize amyloid plaques (green) and cell nuclei (blue), respectively. No differences in plaque load were detected in AD mice with (A,D) or without (B,E) 24-hydroxylase, and no plaques were detected in the absence of the AD transgenes and 24-hydroxylase (C,F).

To determine if rates of plaque accumulation were altered in the absence of 24-hydroxylase, brains from WT/AD and KO/AD male and female animals were collected at 3-month intervals between the ages of 3 and 15 months. Coronal tissue sections were prepared and stained with Congo Red, a dye that selectively binds  $\beta$ -amyloid. Tissues were counterstained with Meyer's hematoxylin for visualization of nuclei. A quantitative determination of plaque load in the cerebral cortex and hippocampus of study animals was made using an unbiased stereological approach. A pilot study was conducted in which plaque load was quantified in a large number (18-21) of tissue sections from each of 6 animals. From this study, we determined that a minimum sampling frequency of 3 evenly-spaced sections per brain region would be necessary to obtain an accurate measurement of plaque burden. The pilot study also revealed that plaque accumulation occurred randomly and evenly throughout the cerebral cortex, whereas these lesions were more abundant in the polymorphic layer of the dentate gyrus than in other regions of the hippocampal formation.

Plaque load determinations were made subsequently in WT/AD and KO/AD male and female mice between the ages of 3 and 15 months. Groups consisted of a minimum of 6 animals of each genotype and sex. The surface area represented by amyloid plaque was quantified using the Cavalieri point counting grid method (76), facilitated by Stereo Investigator software. The Cavalieri probe is a series of grid points with pre-defined spacing (5  $\mu\text{m}$  in the current study).

The surface area of the structures of interest (i.e., amyloid plaques within the cerebral cortex and hippocampus) were proportional to the number of grid points overlaid upon them. Grid points over visible plaques were tallied and converted to a surface area. This area was expressed as a percentage of the total surface area of the examined region (which was defined by a contour drawn along the perimeter of the structure). Percent plaque area was plotted as a function of age (Figure 4). All groups exhibited a linear rate of plaque accumulation over time in both the cerebral cortex and hippocampus. Female mice exhibited plaque formation earlier and accumulated plaques to a greater degree than male mice of the same age (as demonstrated by the upward and leftward shift of the curve in Figure 4B relative to 4A). Plaque accumulation occurred at the same rate and to the same degree in KO/AD male and female mice as observed for their WT/AD male and female littermates at all ages and in both regions examined.

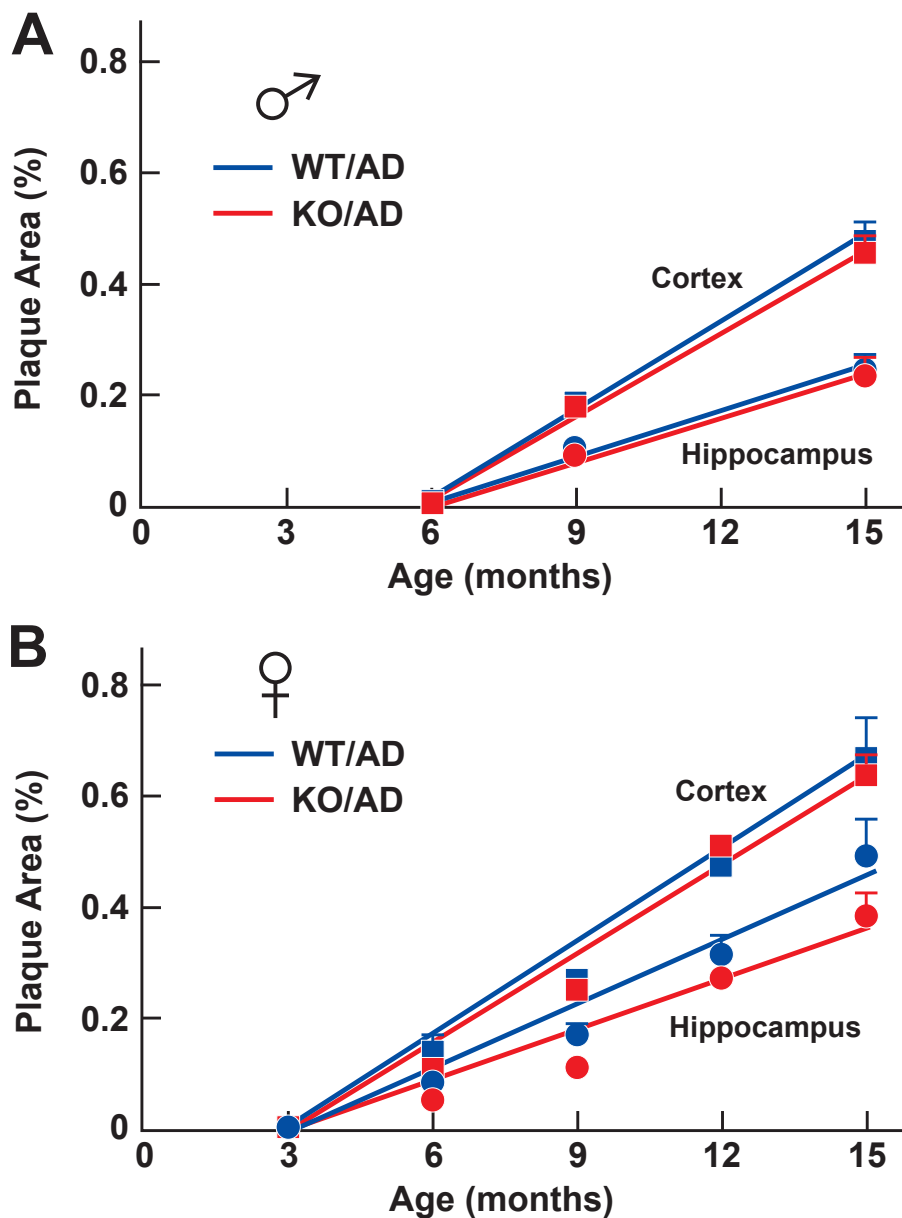


**Figure 4: Amyloid deposition in 24-hydroxylase KO and AD mice.** Coronal sections from the hippocampus and cortex of female (A) and male (B) mice of the indicated genotypes and ages ( $\geq 6$  animals per group) were prepared and stained with Congo Red as described in Materials and Methods. Plaque area was determined by stereology and plotted as a function of the age of the animal. Error bars indicate SEM values.

## **II. Analysis of Proteins Related to Cholesterol Metabolism and Alzheimer's Disease.**

Several reports indicate that levels of 24-hydroxylase are altered in the brains of patients with AD (83). During AD, neurons, the cells that normally express 24-hydroxylase, die. This death may lead to pathological, compensatory expression of the enzyme in astroglial cells, although probably not to a sufficient degree to replace the entire lost pool of 24-hydroxylase. Immunoblotting of brain homogenates from aged female mice revealed no change in 24-hydroxylase protein levels in WT/AD animals when compared to WT littermates, despite the advanced stage of AD pathology (Figure 5, Panel 1). Previous examination of neuropathology in this mouse model of AD has revealed only limited neuritic dystrophy without widespread loss of neurons (84), which may explain why normal levels of 24-hydroxylase are observed in aged WT/AD animals.

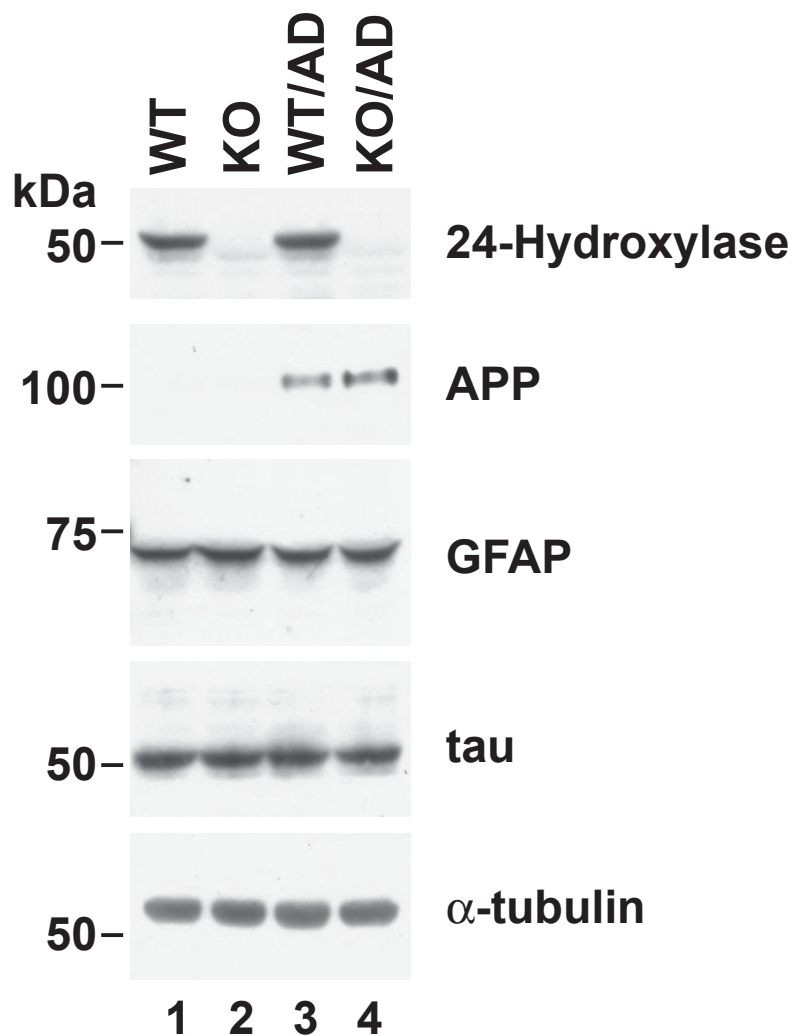


**Figure 5: Protein expression in brains of 24-hydroxylase knockout (KO) and AD mice.** Brain homogenates were prepared from 11- to 13-month old female mice of the indicated genotype and aliquots (35  $\mu$ g of protein) were subjected to immunoblot analysis for the indicated proteins using antibodies as described in Materials and Methods. Film was exposed for 5 to 30 sec. The positions to which standards of known molecular mass ( $\times 10^3$ ) migrated to on the polyacrylamide gel are indicated on the left of each panel.

Astroglial cells are also recruited during states of neurodegeneration, to provide trophic support to damaged neurons. This reactivity, known as astrogliosis, is characterized by an increase in glial fibrillary acidic protein (GFAP) expression in astrocytes. There was no evidence of astrogliosis in aged AD mice, as demonstrated by immunoblotting for GFAP (Figure 5, Panel 3). GFAP expression in WT/AD and KO/AD brains was essentially identical to that seen in the brains of non-transgenic littermates. Additionally, there was no change in the level of GFAP expression in 24-hydroxylase KO mice, consistent with reports that these mice exhibit normal anatomical development within the CNS (20).

Changes in cholesterol metabolism have been demonstrated to affect processing of APP, both *in vivo* and *in vitro* (85). AD mice fed a diet high in cholesterol have been shown to have an increased amyloid plaque load compared with those on a standard diet (86), whereas cholesterol depletion of neurons in culture resulted in a cessation of APP processing to A $\beta$  (87). In the brains of aged AD mice, there was no effect of the absence of 24-hydroxylase on the steady-state level of APP holoprotein (Figure 5, Panel 2), as demonstrated by immunoblotting. This finding suggests that APP expression is unaltered by loss of 24-hydroxylase and the concomitant reduction in brain cholesterol synthesis.

In addition to amyloid plaques, AD patients display characteristic intracellular aggregates consisting of hyperphosphorylated forms of the

microtubule associated protein (MAP) tau. AD mice lacking 24-hydroxylase exhibited no obvious changes in levels of total or phosphorylated tau (Figure 5 and data not shown). The failure of these mice to exhibit neurofibrillary tangles (NFTs), demonstrates that abnormal APP processing and abundant amyloid deposits are insufficient to induce tau pathology in the mouse brain.

### **III. Quantification of A $\beta$ Peptides.**

APP is capable of being processed by three proteases, termed  $\alpha$ -,  $\beta$ - and  $\gamma$ -secretase. Cleavage at the  $\gamma$ -site occurs subsequent to either  $\alpha$ - or  $\beta$ -secretase activity. Processing at the  $\alpha$ -site prior to  $\gamma$ -cleavage produces benign peptide fragments, whereas sequential cleavage at the  $\beta$ - and  $\gamma$ -sites produces pro-amyloidogenic A $\beta$  peptides. The cleaved fragments of APP range from 39 to 43 amino acids in length, with the longer forms demonstrating the propensity to form amyloid deposits. The two most abundant A $\beta$  cleavage products are A $\beta_{40}$  and A $\beta_{42}$ , which are 40- and 42- amino acids in length, respectively. It is thought that a shift toward production of A $\beta_{42}$  over A $\beta_{40}$  is responsible for the neuropathology associated with AD. In support of this idea, mutations in APP and PSEN1/2 that cause early-onset, autosomal-dominant AD lead to a selective increase in production of A $\beta_{42}$ . Patients with Down's syndrome (trisomy 21) have an extra

copy of the APP gene, which gives rise increased production of all A $\beta$  peptides. These subjects begin to exhibit AD neuropathology early in life and develop behavioral symptoms of the disease in the fourth or fifth decade.

To examine APP processing to A $\beta$  peptides in AD mice lacking 24-hydroxylase, peptide levels in tissue homogenates were quantified by enzyme-linked immunosorbent assay (ELISA). Soluble and insoluble (plaque) pools of A $\beta_{40}$  and A $\beta_{42}$  from the cerebral cortex and hippocampus were measured in homogenates from male and female AD animals ranging from 6 to 15-months of age. In cerebral cortical plaques, A $\beta$  levels became detectable in male and female mice at the age of 6 months. This appearance was earlier than in the hippocampus, where levels were not detectable until 9 months of age. Levels of insoluble A $\beta_{40}$  rose rapidly in the cerebral cortex and reached steady-state levels by 12 months (Figure 6A). Females exhibited an earlier rise of A $\beta_{40}$  to steady-state levels than males, but by 15 months, the amount of this peptide in the plaque fraction was the same between the two sexes. Both sexes demonstrated a linear rate of accumulation of insoluble A $\beta_{42}$  in the cerebral cortex with increasing age (Figure 6B). There was no difference in the rate of A $\beta_{42}$  peptide deposition in the cerebral cortex between males and females. Additionally, there were no differences in levels of insoluble A $\beta_{40}$  or A $\beta_{42}$  between KO/AD mice and WT/AD controls at any age examined.

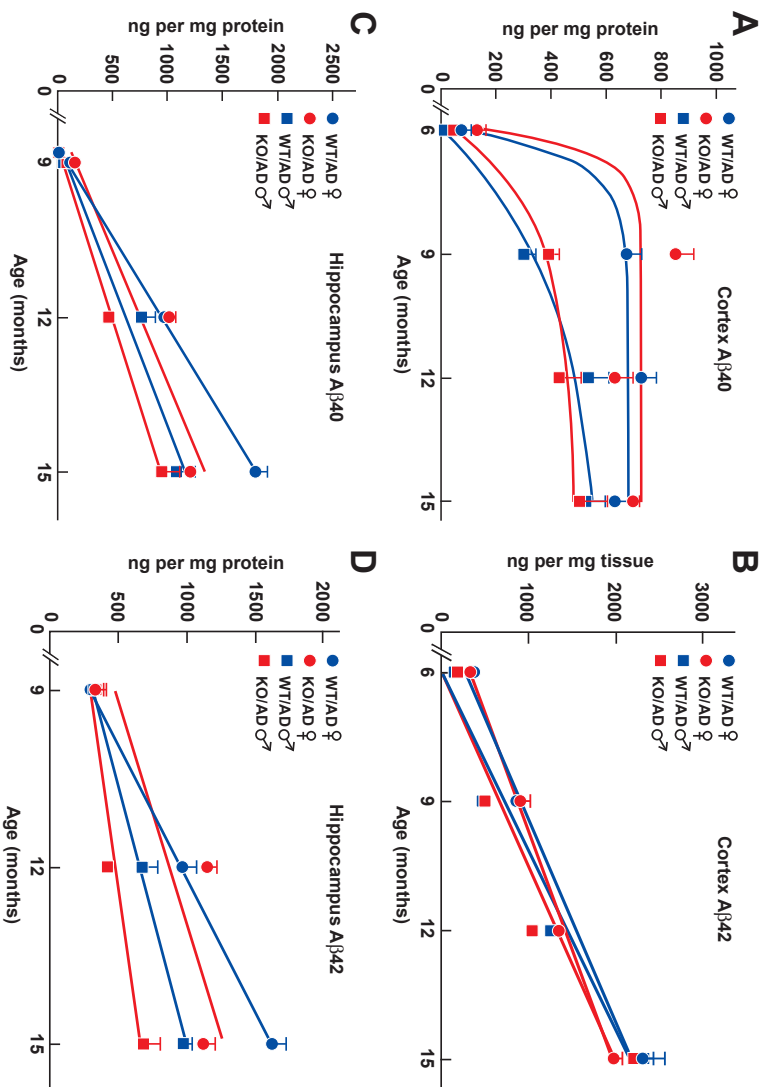


**Figure 6: Insoluble A $\beta$  peptide levels in 24-hydroxylase KO and AD mice.** Cortical (A, B) and hippocampal (C,D) A $\beta$  peptide levels in mice ( $\geq 5$  animals per group) of the indicated genotype, sex, and age were quantified by ELISA as described in Materials and Methods. Tissues were homogenized in RIPA buffer containing protease inhibitors. Insoluble A $\beta$  peptides were isolated by centrifugation and solubilized with 70% formic acid prior to measurement. Error bars indicate SEM values.

By 15 months of age, there was approximately 7-times more  $A\beta_{42}$  than  $A\beta_{40}$  in the cerebral cortex. In contrast, the amount of insoluble  $A\beta_{40}$  in the hippocampus was almost equal to that of  $A\beta_{42}$  by 15 months. In the hippocampus, peptide levels exhibited linear deposition into plaques between 9 and 15 months of age. Females exhibited a trend toward higher levels of both  $A\beta_{40}$  and  $A\beta_{42}$  (Figures 4C and 4D), which achieved statistical significance at 15 months of age in three of the four groups examined (Student's *t* test; WT/AD:  $A\beta_{40}$   $P=0.0073$ ,  $A\beta_{42}$   $P=0.0006$ ; KO/AD:  $A\beta_{40}$  N.S., KO/AD  $A\beta_{42}$   $P=0.0184$ ). Additionally, at 15 months of age, WT/AD males and females demonstrated higher levels of  $A\beta_{40}$  and  $A\beta_{42}$  than their KO/AD counterparts in three of the four groups examined (Student's *t* test; AD male:  $A\beta_{40}$   $P=N.S.$ ,  $A\beta_{42}$   $P=0.0561$ ; AD female:  $A\beta_{40}$   $P=0.0239$ ,  $A\beta_{42}$   $P=0.0059$ ). At 12-months of age, these differences were evident only in males.

$A\beta_{40}$  peptide levels in the detergent-soluble fraction of hippocampal and cerebral cortical brain homogenates were only slightly above the limit of detection at 15 months of age in all groups tested (data not shown). Similarly,  $A\beta_{42}$  peptide was detected exclusively in the plaque fraction, with peptide in the insoluble fraction failing to exceed the level of detection at all ages examined. This is indicative of the propensity of this peptide to accumulate into insoluble aggregates, a property known to be associated with  $A\beta_{42}$ .

#### IV. *In Vivo* Cholesterol Biosynthesis

From the above described quantification studies, we confirmed that WT/AD and KO/AD mice exhibit progressive accumulation of A $\beta$ <sub>42</sub> and amyloid plaque with age. Some *in vitro* studies suggest that A $\beta$  peptides are capable of modulating cholesterol synthesis in cultured neurons (88). To further explore the effects of high levels of A $\beta$  peptides and amyloid plaque on cholesterol metabolism, rates of cholesterol biosynthesis were determined in female animals aged 11-13 months. Females were chosen based on the demonstration that they accumulate amyloid plaque to a greater degree than male AD mice of the same age (Figure 4). Mice were injected with tritiated water, which is capable of freely crossing the blood-brain barrier and of being incorporated into newly synthesized cholesterol. Synthesis of cholesterol in the brain and liver of AD and non-transgenic mice over a 1-hour period was determined. High levels of APP, A $\beta$ , mutant PS1 and amyloid plaque had no effect on cholesterol biosynthesis in the brains of AD mice (Figure 7A). Previous studies have shown that the brain meets cholesterol demand by *de novo* synthesis and that 24-hydroxylase deficient mice exhibit a 40-50% reduction in cholesterol synthesis as a consequence of negative feedback on the mevalonate pathway (19). As expected, there was a reduction in cholesterol synthesis in the brains of KO mice compared to WT. KO/AD mice exhibited a reduction in brain cholesterol synthesis to the same degree as KO.

The defect in cholesterol synthesis in the brains of KO and KO/AD mice was specific to cholesterol metabolism and not a function of global depression of lipid biosynthetic pathways as fatty acid synthesis was the same among all genotypes examined (Figure 7B). Additionally, rates of cholesterol synthesis were indistinguishable in the liver among all genotypes tested, emphasizing that the reduction in cholesterol biosynthesis observed in KO and KO/AD animals was exclusively a phenomenon of the CNS (data not shown).

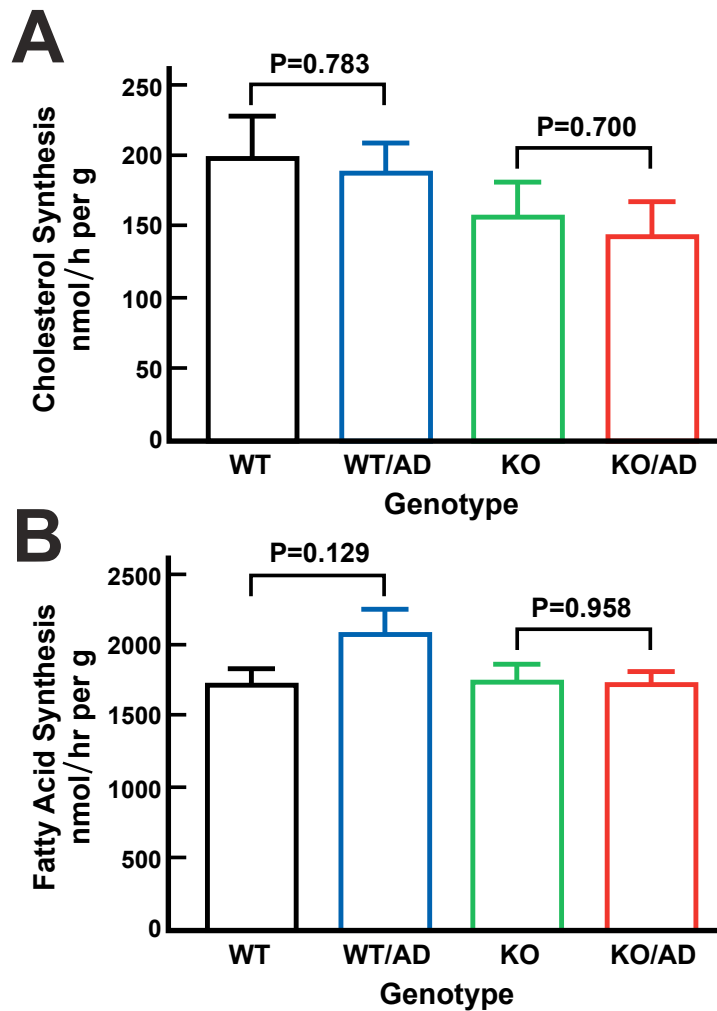


**Figure 7:** *In vivo* synthesis of sterols (A) and fatty acids (B) in 24-hydroxylase KO and AD mice. Mice of the indicated genotypes (11- to 14-month-old females; 10 per group) were maintained on a normal chow diet containing 0.02% cholesterol. On the day of the experiment, each animal was injected peritoneally with 50 mCi of tritium-labeled water and 1 h later, tissues were removed and processed for measurement of radiolabeled sterols and fatty acids as described in Materials and Methods. Student's t-test was performed to assess differences between experimental groups. In (A), KO values were significantly ( $P = 0.022$ ) lower than WT values; KO/AD values were not significantly ( $P = 0.06$ ) lower than WT/AD values. Error bars indicate SEM values.

## V. Survival Study

AD is a progressive, fatal neurodegenerative disorder. Multiple AD transgenic mouse models are known to exhibit premature death beginning prior to the age of 6-months. Studies indicate that amelioration of endogenous tau expression protects mice from death in an APP single-transgenic mouse model, despite having no effect on levels of amyloid plaque or A $\beta$  peptide (89). The transgenic model used in the current study was also susceptible to AD-induced premature death of unidentified cause (personal observation). To examine the role of cholesterol metabolism and 24-hydroxylase in AD mortality, a survival study was performed. Animals of different genotypes were housed in same-sex groups of 2-4 animals per cage and longevity monitored. A minimum of 12 animals was included for each genotype and mice were monitored over a 550-day period. The numbers of female WT/AD mice in the study declined steadily over time, with only about 50% of the animals surviving to the 550-day censor date (Figure 8). Male WT/AD mice demonstrated a similar, though less severe, death rate. Despite the having little to no effect on plaque accumulation and A $\beta$  peptide levels, absence of 24-hydroxylase prolonged life in AD mice. Approximately 90% of KO/AD male and female animals survived past the censor date. Additionally, mice deficient in only one copy of 24-hydroxylase (HET/AD) were

protected from premature death to the same degree as KO/AD mice. All non-transgenic animals exhibited normal rates of survival (data not shown), consistent with observation that 24-hydroxylase KO mice display no outward differences from WT in a variety of physiological read-outs, including life span.

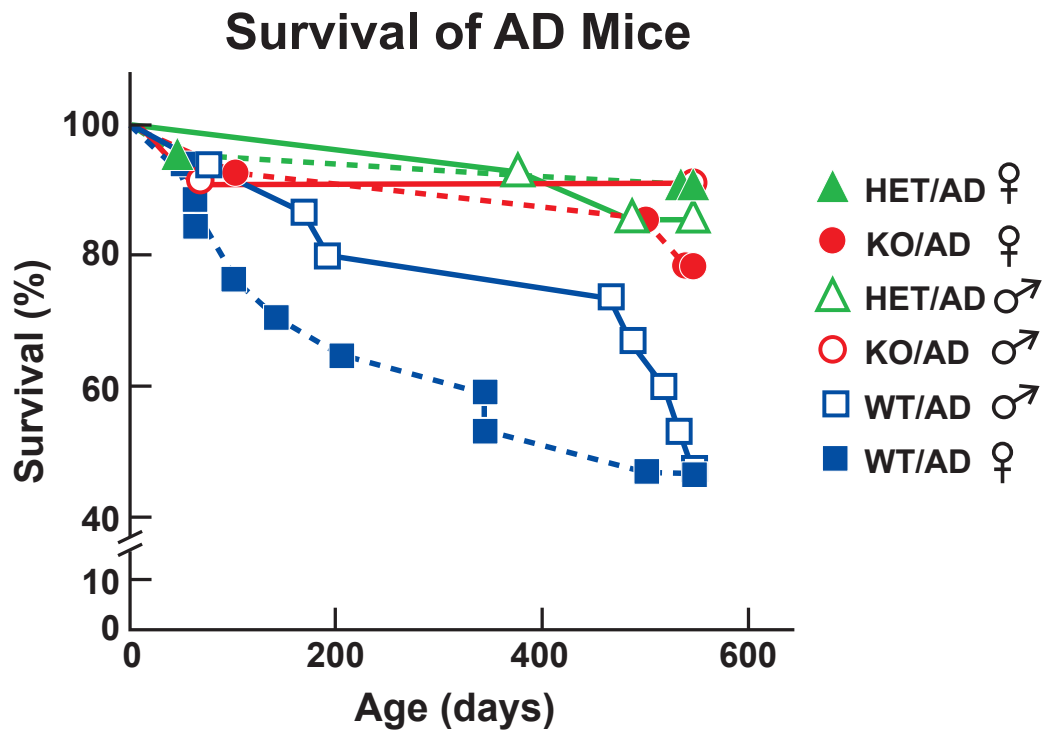


**Figure 8: AD mice live longer in absence of 24-hydroxylase.** Virgin male and female AD mice of the indicated 24-hydroxylase genotypes (HET = +/-, KO = -/-;  $\geq 12$  animals per group) were maintained under standard vivarium conditions (single-sex housing, 2-4 animals per shoe-box; 12-h light/dark cycle) and given food (7001 diet, Harlan Teklad, Madison, WI) and water *ad libitum*. Survival was assessed over a 550-day period and all genotypes were confirmed at death or at the end of the experiment.

## DISCUSSION

The data in the current study indicate that decreasing *de novo* cholesterol synthesis by genetic means does not markedly influence the formation of amyloid plaque in the cortex and hippocampus of a mouse AD model. Additionally, the deposition of amyloid does not have a major effect on cholesterol biosynthetic rates in the central nervous system of these animals. However, the loss of one or more copies of the gene encoding 24-hydroxylase, and presumably the accompanying decrease in cholesterol synthesis, does prolong the life of male and female AD mice.

Several genes with documented or suspected roles in peripheral tissue cholesterol metabolism, including ApoE (90), clusterin (91), and ABCA1 (92, 93), modulate amyloid plaque formation in the mouse brain; however, knockout of any one of these genes, with the exception of clusterin, which has not yet been tested, does not affect cholesterol metabolism in the brain (94). This negative correlation provides support for the hypothesis that the role of ApoE and these other proteins in affecting plaque deposition may not be related to the binding, transport, or metabolism of cholesterol, but rather may involve effects on APP trafficking, APP processing, or A $\beta$  peptide metabolism (95, 96).

In contrast to these findings, 24-hydroxylase knockout mice exhibit a ~50% decrease in *de novo* cholesterol synthesis and a corresponding 50% decrease in cholesterol excretion from the brain (97, 98), but these alterations do not affect rates of amyloid deposition, as judged by Congo red staining. This outcome is similar to that observed in ABCG1 transgenic and knockout mice in which cholesterol synthesis rates are apparently decreased and increased, respectively, but neither of these changes affect APP levels or processing to amyloidogenic A $\beta$  peptides (99). Inasmuch as data from mice can be extrapolated to humans, these outcomes suggest that even if cholesterol-lowering drugs such as statins were able to cross the blood-brain barrier, they would not alter the deposition of amyloid in AD.

An extensive body of literature indicates that acute changes in intracellular cholesterol levels can alter the processing of APP *in vitro* (100), in part by modifying membrane lipid composition, which in turn increases or decreases secretase activity (101-103). Reduced flux of metabolites through the cholesterol biosynthetic pathway in brains of 24-hydroxylase knockout mice did not markedly affect the processing of APP to A $\beta$ 40 and A $\beta$ 42 peptides, implying that levels of secretase activity are similar in WT/AD and KO/AD mice and that intracellular cholesterol levels and distribution are normal in the KO/AD mice. The difference between the *in vivo* results reported here and those from related *in vitro* studies of APP processing may possibly be explained by the harsh

pharmacological treatments used to change intracellular cholesterol levels. Such treatments can temporarily override the intricate regulatory mechanisms that normally maintain membrane cholesterol content within a narrow range (104). In contrast, these regulatory mechanisms are intact in 24-hydroxylase KO mice based on the observation that brain cholesterol levels in the mutant mice are not different from those of WT mice (97, 98). *In vitro* studies also suggest that high concentrations of A $\beta$  peptides can directly modulate cholesterol synthesis in cultured neurons and other cell types (105), whereas here, no effect of extensive amyloid accumulation was observed on cholesterol synthesis *in vivo*. These disparate findings may reflect differences in rates or extent of A $\beta$  peptide accumulation or polymerization.

In humans, AD is a progressive, fatal neurodegenerative disorder and some mouse models, such as the one used in the current study, recapitulate the premature death associated with the human disease. Interestingly, loss of one or more 24-hydroxylase alleles confers a normal lifespan to both male and female animals. Although there are potential alternative explanations to these findings, such as the small number of animals in each experimental group and the possibility of exposure to mouse hepatitis virus due to an outbreak that occurred during the course of the study, the observation that increased longevity was observed in four experimental groups (HET/AD males and females, and KO/AD males and females) suggests that loss of this gene does confer a true survival

advantage. 24-hydroxylase knockout mice exhibit a co-dominant phenotype, with heterozygotes manifesting intermediate levels of reduced cholesterol synthesis and excretion (R. W. Halford, unpublished observations). This phenotypic effect in turn indicates that the increase in lifespan observed in 24-hydroxylase heterozygous and knockout AD mice may be linked to the alteration in cholesterol metabolism.

Taken together, these data suggest that reducing cholesterol metabolism in the brain may protect against the deleterious effects of AD, independent of changes in plaque burden and A $\beta$  peptide production. In the future, it may be of interest to determine the underlying molecular and cellular changes responsible for premature death in AD transgenic mice. It has been shown that A $\beta$  peptide can trigger non-convulsive, aberrant excitatory neuronal activity in the cortex and hippocampus of AD transgenic mice (106), which may lead to compensatory synaptic remodeling and subsequent functional impairment of neuronal networks.

Targeted deletion of the microtubule associated protein tau, a protein that deposits intraneuronally (as neurofibrillary tangles) in the brains of humans with AD, protects AD transgenic mice against the lethal effects of A $\beta$  (89). Administration of agents that block  $\gamma$ -aminobutyric acid (GABA) inhibitory signals have been shown to potentiate the excitotoxic effects of A $\beta$  in mice, an effect that is mitigated by absence of one or both copies of tau (89). Additionally, loss of tau protects against excitotoxicity induced by the glutamate receptor

agonist kainate in the absence of pathological levels of A $\beta$  (89). However, like mice lacking even one copy of 24-hydroxylase, tau deficient mice are cognitively impaired and are not able to perform as well as WT counterparts on tasks that require motor and contextual learning (107). As observed with loss of tau, 24-hydroxylase HET/AD and KO/AD mice escape the lethal effects of high levels of A $\beta$ , whereas WT/AD male and female mice do not. It is conceivable that depression of neuronal excitability or synaptic potentiation conferred by absence of either of these proteins underlies the protective effect of these mutations on premature death and that the same synaptic mechanisms are responsible for the cognitive insufficiency observed in these animals. Neuronal excitability in 24-hydroxylase KO mice could be tested using pharmacological agents to manipulate synaptic activity. Mice lacking 24-hydroxylase would be expected to exhibit resistance to hyperexcitability induced by GABA agonists in the presence of A $\beta$  or to kainate in the non-transgenic state.

At present, the value of these findings with regard to human disease is unclear. Improving long-term survival and quality of life of patients with AD is of central importance to the scientific and medical communities. Based on results from the current study, disruption of 24-hydroxylase may provide a route toward achieving one of these goals. Of major concern would be the effects of such an intervention on human cognition. Specifically, chronic disruption of the cholesterol efflux pathway may lead to profound impairments in mental function,

an unacceptable outcome, particularly in patients already affected by a debilitating neurodegenerative disorder. In order to address this issue, further investigation would be necessary. Studies using the available model suggest that the phenotype observed in 24-hydroxylase KO mice is the result of a deficiency of metabolites of the cholesterol biosynthetic pathway, rather than a developmental defect. An inducible 24-hydroxylase conditional knock-out mouse model could be generated to address this issue. Expression of the protein could be disrupted at various ages and stages of AD to determine the extent to which cognition is subsequently impaired. LTP deficits can be rescued in acute hippocampal slices from 24-hydroxylase KO mice by administration of geranylgeraniol, a metabolite in the cholesterol and isoprenoid biosynthetic pathways. The role of prolonged treatment with geranylgeraniol in improving cognition and modulating the neuroprotective effects of loss of 24-hydroxylase *in vivo* in the context of pathological levels of A $\beta$  would also need to be explored.

Finally, it is important to consider that although animal models of AD recapitulate major features of the disease, including amyloid plaque deposition and premature death, these animals do not provide a complete model of the human disease. In humans, death from AD occurs subsequent to widespread neurodegeneration, amyloid deposition, glial activation, tau hyperphosphorylation and intracellular formation of neurofibrillary tangles over the course of decades. Many of these features are not reproduced spontaneously in AD mouse models.

Additionally, human pathology occurs most frequently in the absence of mutations in APP and PSEN1, two proteins that are expressed in mutant forms and at very high levels in animal models in order to drive amyloid plaque deposition. Before the role of genetic or pharmacological manipulations, including disruption of 24-hydroxylase, on the progression of human AD can be projected, it will be of value to examine them in the context of a more complete model of AD. Further insight into the molecular events underlying neuronal changes in the brains of individuals with AD will undoubtedly yield more faithful animal models of the disease, thus providing even more powerful tools with which to unwind this disease – a disease that has challenged physicians and scientists for more than 100 years.

## BIBLIOGRAPHY

1. Mc MJ & Brigden WW (1950) *Annu Rev Med* **1**, 61-78.
2. Goldstein JL & Brown MS (1973) *Proc Natl Acad Sci U S A* **70**, 2804-2808.
3. Brown MS & Goldstein JL (1979) *Proc Natl Acad Sci U S A* **76**, 3330-3337.
4. Goldstein JL, DeBose-Boyd RA, & Brown MS (2006) *Cell* **124**, 35-46.
5. Ikonen E (2008) *Nat Rev Mol Cell Biol* **9**, 125-138.
6. Dietschy JM & Turley SD (2001) *Curr Opin Lipidol* **12**, 105-112.
7. Dietschy JM & Turley SD (2004) *J Lipid Res* **45**, 1375-1397.
8. Goldstein JL & Brown MS (1990) *Nature* **343**, 425-430.
9. Brown MS, Dana SE, & Goldstein JL (1973) *Proc Natl Acad Sci U S A* **70**, 2162-2166.
10. Brown MS & Goldstein JL (2004) *Atheroscler Suppl* **5**, 57-59.
11. Russell DW (2003) *Annu Rev Biochem* **72**, 137-174.
12. Lutjohann D, Breuer O, Ahlborg G, Nennesmo I, Siden A, Diczfalusy U, & Bjorkhem I (1996) *Proc Natl Acad Sci U S A* **93**, 9799-9804.
13. Ercoli A, Di Frisco S, & De Ruggieri P (1953) *Boll Soc Ital Biol Sper* **29**, 494-497.

14. Bjorkhem I, Lutjohann D, Breuer O, Sakinis A, & Wennmalm A (1997) *J Biol Chem* **272**, 30178-30184.
15. Norlin M, Toll A, Bjorkhem I, & Wikvall K (2000) *J Lipid Res* **41**, 1629-1639.
16. Lund EG, Guileyardo JM, & Russell DW (1999) *Proc Natl Acad Sci U S A* **96**, 7238-7243.
17. Dhar AK, Teng JI, & Smith LL (1973) *J Neurochem* **21**, 51-60.
18. Otyepka M, Skopalik J, Anzenbacherova E, & Anzenbacher P (2007) *Biochim Biophys Acta* **1770**, 376-389.
19. Lund EG, Xie C, Kotti T, Turley SD, Dietschy JM, & Russell DW (2003) *J Biol Chem* **278**, 22980-22988.
20. Kotti TJ, Ramirez DM, Pfeiffer BE, Huber KM, & Russell DW (2006) *Proc Natl Acad Sci U S A* **103**, 3869-3874.
21. Repa JJ & Mangelsdorf DJ (2000) *Annu Rev Cell Dev Biol* **16**, 459-481.
22. Janowski BA, Willy PJ, Devi TR, Falck JR, & Mangelsdorf DJ (1996) *Nature* **383**, 728-731.
23. Grundy SM (1997) *Arch Intern Med* **157**, 1177-1184.
24. Hegele RA (2001) *Am J Hum Genet* **69**, 1161-1177.
25. Brown MS & Goldstein JL (1977) *Am J Clin Nutr* **30**, 975-978.
26. Vance JE, Hayashi H, & Karten B (2005) *Semin Cell Dev Biol* **16**, 193-212.

27. Infante RE, Radhakrishnan A, Abi-Mosleh L, Kinch LN, Wang ML, Grishin NV, Goldstein JL, & Brown MS (2008) *J Biol Chem* **283**, 1064-1075.
28. German DC, Liang CL, Song T, Yazdani U, Xie C, & Dietschy JM (2002) *Neuroscience* **109**, 437-450.
29. Liu Y, Wu YP, Wada R, Neufeld EB, Mullin KA, Howard AC, Pentchev PG, Vanier MT, Suzuki K, & Proia RL (2000) *Hum Mol Genet* **9**, 1087-1092.
30. Wolozin B (2003) *Arch Neurol* **60**, 16-18.
31. Lutjohann D, Papassotiropoulos A, Bjorkhem I, Locatelli S, Bagli M, Oehring RD, Schlegel U, Jessen F, Rao ML, von Bergmann K, *et al.* (2000) *J Lipid Res* **41**, 195-198.
32. Vega GL & Weiner MF (2007) *J Mol Neurosci* **33**, 51-55.
33. Bjorkhem I, Lutjohann D, Diczfalusy U, Stahle L, Ahlborg G, & Wahren J (1998) *J Lipid Res* **39**, 1594-1600.
34. Mahley RW, Innerarity TL, Rall SC, Jr., & Weisgraber KH (1984) *J Lipid Res* **25**, 1277-1294.
35. Mahley RW, Weisgraber KH, & Huang Y (2006) *Proc Natl Acad Sci U S A* **103**, 5644-5651.

36. Zannis VI, Breslow JL, Utermann G, Mahley RW, Weisgraber KH, Havel RJ, Goldstein JL, Brown MS, Schonfeld G, Hazzard WR, *et al.* (1982) *J Lipid Res* **23**, 911-914.
37. Scriver CR (2001) *The Metabolic and Molecular Bases of Inherited Disease* (McGraw-Hill, New York).
38. Mahley RW & Innerarity TL (1983) *Biochim Biophys Acta* **737**, 197-222.
39. Skene JH & Shooter EM (1983) *Proc Natl Acad Sci U S A* **80**, 4169-4173.
40. Ignatius MJ, Gebicke-Harter PJ, Skene JH, Schilling JW, Weisgraber KH, Mahley RW, & Shooter EM (1986) *Proc Natl Acad Sci U S A* **83**, 1125-1129.
41. Beffert U, Nematollah Farsian F, Masiulis I, Hammer RE, Yoon SO, Giehl KM, & Herz J (2006) *Curr Biol* **16**, 2446-2452.
42. Trommsdorff M, Gotthardt M, Hiesberger T, Shelton J, Stockinger W, Nimpf J, Hammer RE, Richardson JA, & Herz J (1999) *Cell* **97**, 689-701.
43. Beffert U, Durudas A, Weeber EJ, Stolt PC, Giehl KM, Sweatt JD, Hammer RE, & Herz J (2006) *J Neurosci* **26**, 2041-2052.
44. Strittmatter WJ, Saunders AM, Schmechel D, Pericak-Vance M, Enghild J, Salvesen GS, & Roses AD (1993) *Proc Natl Acad Sci U S A* **90**, 1977-1981.

45. Corder EH, Saunders AM, Strittmatter WJ, Schmechel DE, Gaskell PC, Small GW, Roses AD, Haines JL, & Pericak-Vance MA (1993) *Science* **261**, 921-923.
46. Weisgraber KH & Mahley RW (1996) *FASEB J* **10**, 1485-1494.
47. Price DL, Tanzi RE, Borchelt DR, & Sisodia SS (1998) *Annu Rev Genet* **32**, 461-493.
48. Poirier J, Davignon J, Bouthillier D, Kogan S, Bertrand P, & Gauthier S (1993) *Lancet* **342**, 697-699.
49. Maurer K, Volk S, & Gerbaldo H (1997) *Lancet* **349**, 1546-1549.
50. Perusini G (1909) *Histologische un Histopathologishce Arbeiten*, 297-351.
51. Tanzi RE & Bertram L (2005) *Cell* **120**, 545-555.
52. Glenner GG & Wong CW (1984) *Biochem Biophys Res Commun* **120**, 885-890.
53. Glenner GG & Wong CW (1984) *Biochem Biophys Res Commun* **122**, 1131-1135.
54. Heston LL, Matri AR, Anderson VE, & White J (1981) *Arch Gen Psychiatry* **38**, 1085-1090.
55. Heyman A, Wilkinson WE, Hurwitz BJ, Schmechel D, Sigmon AH, Weinberg T, Helms MJ, & Swift M (1983) *Ann Neurol* **14**, 507-515.

56. St George-Hyslop PH, Tanzi RE, Polinsky RJ, Haines JL, Nee L, Watkins PC, Myers RH, Feldman RG, Pollen D, Drachman D, *et al.* (1987) *Science* **235**, 885-890.
57. Goate A, Chartier-Harlin MC, Mullan M, Brown J, Crawford F, Fidani L, Giuffra L, Haynes A, Irving N, James L, *et al.* (1991) *Nature* **349**, 704-706.
58. Chartier-Harlin MC, Crawford F, Houlden H, Warren A, Hughes D, Fidani L, Goate A, Rossor M, Roques P, Hardy J, *et al.* (1991) *Nature* **353**, 844-846.
59. Heber S, Herms J, Gajic V, Hainfellner J, Aguzzi A, Rulicke T, von Kretschmar H, von Koch C, Sisodia S, Tremml P, *et al.* (2000) *J Neurosci* **20**, 7951-7963.
60. Guenette S, Chang Y, Hiesberger T, Richardson JA, Eckman CB, Eckman EA, Hammer RE, & Herz J (2006) *EMBO J* **25**, 420-431.
61. Ring S, Weyer SW, Kilian SB, Waldron E, Pietrzik CU, Filippov MA, Herms J, Buchholz C, Eckman CB, Korte M, *et al.* (2007) *J Neurosci* **27**, 7817-7826.
62. Yang P, Baker KA, & Hagg T (2006) *Prog Neurobiol* **79**, 73-94.
63. Haass C (2004) *EMBO J* **23**, 483-488.
64. Shah S, Lee SF, Tabuchi K, Hao YH, Yu C, LaPlant Q, Ball H, Dann CE, 3rd, Sudhof T, & Yu G (2005) *Cell* **122**, 435-447.

65. Brown MS, Ye J, Rawson RB, & Goldstein JL (2000) *Cell* **100**, 391-398.
66. Hardy J & Allsop D (1991) *Trends Pharmacol Sci* **12**, 383-388.
67. Yankner BA, Duffy LK, & Kirschner DA (1990) *Science* **250**, 279-282.
68. Tanzi RE, Vaula G, Romano DM, Mortilla M, Huang TL, Tupler RG, Wasco W, Hyman BT, Haines JL, Jenkins BJ, *et al.* (1992) *Am J Hum Genet* **51**, 273-282.
69. (1995) *Nat Genet* **11**, 219-222.
70. Sherrington R, Rogaev EI, Liang Y, Rogaeva EA, Levesque G, Ikeda M, Chi H, Lin C, Li G, Holman K, *et al.* (1995) *Nature* **375**, 754-760.
71. van Marum RJ (2008) *Fundam Clin Pharmacol* **22**, 265-274.
72. Menge T, Hartung HP, & Stuve O (2005) *Nat Rev Neurosci* **6**, 325-331.
73. Cordle A, Koenigsnecht-Talboo J, Wilkinson B, Limpert A, & Landreth G (2005) *J Biol Chem* **280**, 34202-34209.
74. Jankowsky JL, Fadale DJ, Anderson J, Xu GM, Gonzales V, Jenkins NA, Copeland NG, Lee MK, Younkin LH, Wagner SL, *et al.* (2004) *Hum Mol Genet* **13**, 159-170.
75. Mullan M, Crawford F, Axelman K, Houlden H, Lilius L, Winblad B, & Lannfelt L (1992) *Nat Genet* **1**, 345-347.
76. Mouton PR & ebrary Inc. (2002) (Johns Hopkins University Press, Baltimore), pp. x, 214 p.
77. Gundersen HJ & Osterby R (1981) *J Microsc* **121**, 65-73.

78. Hooper NM (2000) *Alzheimer's disease : methods and protocols* (Humana Press, Totowa, N.J.).
79. Andersen JM & Dietschy JM (1979) *J Lipid Res* **20**, 740-752.
80. Jeske DJ & Dietschy JM (1980) *J Lipid Res* **21**, 364-376.
81. Sambrook J & Russell DW (2001) *Molecular cloning : a laboratory manual* (Cold Spring Harbor Laboratory Press, Cold Spring Harbor, N.Y.).
82. Ramirez DM, Andersson S, & Russell DW (2008) *J Comp Neurol* **507**, 1676-1693.
83. Bogdanovic N, Bretillon L, Lund EG, Diczfalusy U, Lannfelt L, Winblad B, Russell DW, & Bjorkhem I (2001) *Neurosci Lett* **314**, 45-48.
84. Perez SE, Dar S, Ikonomovic MD, DeKosky ST, & Mufson EJ (2007) *Neurobiol Dis* **28**, 3-15.
85. Howland DS, Trusko SP, Savage MJ, Reaume AG, Lang DM, Hirsch JD, Maeda N, Siman R, Greenberg BD, Scott RW, *et al.* (1998) *J Biol Chem* **273**, 16576-16582.
86. Refolo LM, Malester B, LaFrancois J, Bryant-Thomas T, Wang R, Tint GS, Sambamurti K, Duff K, & Pappolla MA (2000) *Neurobiol Dis* **7**, 321-331.
87. Simons M, Keller P, De Strooper B, Beyreuther K, Dotti CG, & Simons K (1998) *Proc Natl Acad Sci U S A* **95**, 6460-6464.

88. Grimm MO, Grimm HS, Patzold AJ, Zinser EG, Halonen R, Duering M, Tschape JA, De Strooper B, Muller U, Shen J, *et al.* (2005) *Nat Cell Biol* **7**, 1118-1123.
89. Roberson ED, Scarce-Levie K, Palop JJ, Yan F, Cheng IH, Wu T, Gerstein H, Yu GQ, & Mucke L (2007) *Science* **316**, 750-754.
90. Bales KR, Verina T, Dodel RC, Du Y, Altstiel L, Bender M, Hyslop P, Johnstone EM, Little SP, Cummins DJ, *et al.* (1997) *Nat Genet* **17**, 263-264.
91. DeMattos RB, O'dell MA, Parsadanian M, Taylor JW, Harmony JA, Bales KR, Paul SM, Aronow BJ, & Holtzman DM (2002) *Proc. Natl. Acad. Sci. U.S.A.* **99**, 10843-10848.
92. Wahrle SE, Jiang H, Parsadanian M, Hartman RE, Bales KR, Paul SM, & Holtzman DM (2005) *J. Biol. Chem.* **280**, 43236-43242.
93. Wahrle SE, Jiang H, Parsadanian M, Kim J, Li A, Knoten A, Jain S, Hirsch-Reinshagen V, Wellington CL, Bales KR, *et al.* (2008) *J. Clin. Invest.* **118**, 671-682.
94. Quan G, Xie C, Dietschy JM, & Turley SD (2003) *Brain Res. Dev. Brain Res.* **146**, 87-98.
95. DeMattos RB (2004) *J. Mol. Neurosci.* **23**, 255-262.
96. Jiang Q, Lee CY, Mandrekar S, Wilkinson B, Cramer P, Zelcer N, Mann K, Lamb B, Willson TM, Collins JL, *et al.* (2008) *Neuron* **58**, 681-693.

97. Lund EG, Xie C, Kotti T, Turley SD, Dietschy JM, & Russell DW (2003) *J. Biol. Chem.* **278**, 22980-22988.
98. Xie C, Lund EG, Turley SD, Russell DW, & Dietschy JM (2003) *J. Lipid Res.* **44**, 1780-1789.
99. Burgess BL, Parkinson PF, Racke MM, Hirsch-Reinshagen V, Fan J, Wong C, Stukas S, Theroux L, Chan JY, Donkin J, *et al.* (2008) *J. Lipid Res.* **49**, 1254-1267.
100. Wolozin B (2004) *Neuron* **41**, 7-10.
101. Bodovitz S & Klein WL (1996) *J. Biol. Chem.* **271**, 4436-4440.
102. Kalvodova L, Kahya N, Schwille P, Eehalt R, Verkade P, Drechsel D, & Simons K (2005) *J. Biol. Chem.* **280**, 36815-36823.
103. Osenkowski P, Ye W, Wang R, Wolfe MS, & Selkoe DJ (2008) *J. Biol. Chem.* **283**, 22529-22540.
104. Goldstein JL, DeBose-Boyd RA, & Brown MS (2006) *Cell* **124**, 35-46.
105. Grimm MO, Grimm HS, Pätzold AJ, Zinser EG, Halonen R, Duering M, Tschäpe JA, De Strooper B, Müller U, Shen J, *et al.* (2005) *Nat. Cell Biol.* **7**, 1118-1123.
106. Palop JJ, Chin J, Roberson ED, Wang J, Thwin MT, Bien-Ly N, Yoo J, Ho KO, Yu GQ, Kreitzer A, *et al.* (2007) *Neuron* **55**, 697-711.
107. Ikegami S, Harada A, & Hirokawa N (2000) *Neurosci Lett* **279**, 129-132.